BNL-91226-2010-JA

SOOT PARTICLE STUDIES - INSTRUMENT INTER-COMPARISON – PROJECT OVERVIEW

E. S. Cross[1,2], T. B. Onasch[1,2], A. Ahern[1,2], W. Wrobel[1], J. G. Slowik[3], J. Olfert[4,12], D. A. Lack[5,14], P. Massoli[2,5], C. D. Cappa[6], J. Schwarz[5], J. R. Spackman[5], D. W. Fahey[5], A. Sedlacek[4], A. Trimborn[2], J. T. Jayne[2], A. Freedman[2], L. R. Williams[2], N. L. Ng[2], C. Mazzoleni[7,13], M. Dubey[7], B. Brem[8], G. Kok[9], R. Subramanian[9], S. Freitag[10], A. Clarke[10], D. Thornhill[11], L. Marr[11], C. E. Kolb[2], D. R. Worsnop[2], and P. Davidovits[1]

[1] *Chemistry Department, Boston College, Chestnut Hill, MA*
[2] *Aerodyne Research, Inc., Billerica, MA*
[3] *Chemistry Department, University of Toronto, Toronto, CA*
[4] *Brookhaven National Laboratory, Upton, NY*
[5] *NOAA Earth System Research Laboratory, Chemical Sciences Division, Boulder, CO*
[6] *Department of Civil and Environmental Engineering, University of California, Davis, CA*
[7] *Los Alamos National Laboratory, Los Alamos, NM*
[8] *Department of Civil and Environmental Engineering, University of Illinois, Urbana, IL*
[9] *Droplet Measurement Technologies, Boulder, CO*
[10] *Department of Oceanography, University of Hawaii, Honolulu, HI*
[11] *Department of Civil and Environmental Engineering, Virginia Tech, Blacksburg, VA*
[12] *Department of Mechanical Engineering, University of Alberta, Edmonton, Alberta, Canada*
[13] *Department of Physics, Michigan Technological University, Houghton, MI*
[14] *Cooperative Institute for Research of the Environmental Sciences, University of Colorado, Boulder, CO*

March 2010

Accepted for publication in
Atmos. Sci. Technol.

Environmental Sciences Department/Atmospheric Sciences Division

Brookhaven National Laboratory
P.O. Box 5000
Upton, NY 11973-5000
www.bnl.gov

DISCLAIMER

ABSTRACT

An inter-comparison study of instruments designed to measure the microphysical and optical properties of soot particles was completed. The following mass-based instruments were tested: Couette Centrifugal Particle Mass Analyzer (CPMA), Time-of-Flight Aerosol Mass Spectrometer - Scanning Mobility Particle Sizer (AMS-SMPS), Single Particle Soot Photometer (SP2), Soot Particle-Aerosol Mass Spectrometer (SP-AMS) and Photoelectric Aerosol Sensor (PAS2000CE). Optical instruments measured absorption (photoacoustic, interferometric and filter-based), scattering (in situ) and extinction (light attenuation within an optical cavity). The study covered an experimental matrix consisting of 318 runs that systematically tested the performance of instruments across a range of parameters including: fuel equivalence ratio ($1.8 \leq \phi \leq 5$), particle shape (mass-mobility exponent (D_{fm}), $2.0 \leq D_{fm} \leq 3.0$), particle mobility size ($30 \leq d_m \leq 300$ nm), black carbon mass ($0.07 \leq m_{BC} \leq 4.2$ fg) and particle chemical composition. In selected runs, particles were coated with sulfuric acid or dioctyl sebacate (DOS) ($0.5 \leq \Delta r_{ve} \leq 201$ nm) where Δr_{ve} is the change in the volume equivalent radius due to the coating material. The effect of non-absorbing coatings on instrument response was determined. Changes in the morphology of fractal soot particles were monitored during coating and denuding processes and the effect of particle shape on instrument response was determined. The combination of optical and mass based measurements was used to determine the mass specific absorption coefficient for denuded soot particles. The single scattering albedo of the particles was also measured. An overview of the experiments and sample results are presented.

1. Introduction.

Soot particles that contain black carbon (BC) are emitted during combustion of fossil and biomass fuels. Air borne aerosol particles containing BC directly absorb sunlight, heating the particles and the surrounding atmosphere (*Schwartz and Buseck*, 2000). Most other aerosol particles predominately scatter sunlight cooling the surface and lower atmosphere (*Ramanathan et al.* 2001). It has been estimated that the direct radiative effect of BC is the second-most important contributor to global warming after absorption by CO_2 (*Jacobson*, 2001). Ongoing studies continue to underscore the climate forcing importance of BC (*Ramanathan and Carmichael,* 2008; *Grieshop*, 2009; *Rypdal*, 2009; *Ramanathan and Feng,* 2009). However, estimates of BC climate effects are highly uncertain in large part because of the physical and chemical complexity of particles containing BC.

Freshly emitted soot particles are typically fractal hydrophobic aggregates consisting of black carbon spherules with diameters in the range of ~20-40 nm (*Seinfeld and Pandis*, 2006; *Chakrabarty et al.* 2009). This complex morphology makes quantitative measurement of BC particle properties particularly challenging (*Park et al.* 2003; *Chakrabarty et al.* 2006). Fractal BC cores are often coated with aliphatic organic compounds from lubricating oil and unburned fuel (*Canagaratna et al.* 2004; *Sakurai et al.* 2003; *Kittelson,* 1998) as well as polycyclic aromatic hydrocarbons (PAHs) (*Marr et al.* 2004; *Jiang et al.* 2005), depending on the fuel content and combustion conditions. Sulfuric acid has also been detected in diesel and aircraft-emitted soot particles (*Curtius et al.* 1998; *Onasch et al.* 2009). With increasing atmospheric residence time, soot particles acquire additional coatings through deposition of semivolatile

atmospheric species or coagulation with pre-existing particles. Such processes transform the morphological, chemical and optical properties as well as the cloud condensation nuclei (CCN) activity, of the soot particles, further complicating parameterization of their climate effects. To fully characterize BC-containing particles one must measure, in real-time, the mass of BC in the particles as well as the optical properties (absorption, scattering and extinction) of the particles.

The recent development of aerosol mass spectrometers now allows real-time determination of the size and composition of aerosol particle ensembles (*Murphy,* 2006; *Canagaratna et al.* 2007). Instruments have also been developed to provide real-time measurements of the mass and optical properties of BC-containing particles. Some mass-based instruments include the Single Particle Soot Photometer (SP2) (*Stephens et al.* 2003; *Schwarz et al.* 2006) and the Couette Centrifugal Particle Mass Analyzer (CPMA) (*Olfert and Collings,* 2005). Common techniques for aerosol optical property measurements include: cavity ring down spectroscopy (*Smith and Atkinson* 2001; *Bulatov et al.* 2002; *Atkinson* 2003; *Strawa et al.* 2003; *Pettersson et al.* 2004; *Moosmüller et al.* 2005) for aerosol extinction; nephelometry (*Heintzenberg and Charlson*, 1996 and references therein) for aerosol scattering; photo-acoustic (*Arnott et al.* 1999; *Lack et al.* 2006), interferometry (*Davis*, 1980; *Campillo and Lin,* 1981; *Fluckiger et al.* 1985) and real-time filter-based methods such as the aethalometer (*Hansen et al.* 1984), particle soot absorption photometer (PSAP) (*Bond et al.* 1999) and multi angle absorption photometer (MAAP) (*Petzold et al.* 2004) for aerosol absorption. Combining measurements from these instruments has the potential to provide real-time/near real-time quantitative physical, chemical and optical characterization of BC-containing aerosol particles. To achieve this potential, instrument performance must be validated using a wide range of BC containing particles with known properties.

Inter-comparison studies under controlled conditions (known particle mass, size, number and composition) are an indispensable step in the instrument validation process. Inter-comparison measurements are necessary if one is to attain the degree of understanding required to reduce the large uncertainties associated with the effects of BC-containing aerosol particles on climate.

Several previous inter-comparison studies of BC measurements have been conducted (See *Slowik et al.* 2007a and references therein). Two inter-comparison studies have been completed in Boston College laboratories, one in May 2005 (*Slowik et al.* 2007a) and another in July of 2008 – the subject of the present manuscript. The key component of the Boston College laboratory apparatus is a well-characterized soot generation/sampling system developed by the Boston College/Aerodyne Research, Inc. group (*Slowik et al.* 2007a). The soot particle generation/sampling source used in the current inter-comparison study is improved relative to our previous work. The improved system is capable of providing stable, monomodal soot distributions across a size range of $30 \leq d_m \leq 300$ nm. The new soot sampling system was also able to provide a significantly higher total particle flow making it possible to simultaneously measure properties of soot particles with up to 18 instruments (total flow rate ~ 22 L/min).

Twenty-six scientists representing 12 institutions participated in the inter-comparison study operating 7 mass-based and 9 optically-based instruments; filter samples for Scanning Electron Microscopy (SEM) and Organic Carbon Elemental Carbon (OCEC) analyses were also obtained. The study covered an experimental matrix consisting of 318 runs that systematically tested the performance of instruments across a wide range of parameters including: fuel equivalence ratio ($1.8 \leq \phi \leq 5$), particle shape (mass-mobility exponent $2.0 \leq D_{fm} \leq 3.0$), particle mobility size ($30 \leq d_m \leq 300$ nm), black carbon mass ($0.07 \leq m_{BC} \leq 4.2$ fg) and particle chemistry

and density (changed via coatings). In select runs, particles were coated with a known thickness of sulfuric acid or dioctyl sebacate (DOS) ($0.5 \leq \Delta r_{ve} \leq 201$ nm).

Highlights of the inter-comparison study include: CPMA mass measurements of coated soot particles and their corresponding soot cores, SMPS-AMS / CPMA total mass measurement comparisons, multiple measurements of the mass specific absorption coefficient for different types of soot particles, mass specific absorption enhancement (E_{abs}) as a function of coating type and thickness, wavelength-dependent measurements of absorption, scattering, and extinction as a function of soot particle type, and particle shape determination as a function of fuel-to-air ratio. Collapse of particle shape was observed in the coating-denuding process. In addition to flame-generated soot, black carbon particles obtained by atomizing fullerene soot, oxidized flame soot, Regal black toner, and Aquadag paint were also characterized. In this manuscript, we only present results obtained for flame-generated soot particles. The intent of the article is to explain the goals of the study, to provide an overview of the experimental methodology, and to illustrate the type of data obtained by presenting key sample results for selected instrument inter-comparison experiments. Accordingly, descriptions of the specific instruments are restricted to providing the basic operating principles necessary to understand the nature and range of information a given instrument can provide and what aspects of the data provided can be meaningfully inter-compared with other instruments. More detailed results and discussions related to specific instruments will be provided in subsequent publications.

2. Inter-compared Instruments and Scope of the Study.

We divide the instruments tested into two categories: mass-based and optically-based, listed in Tables 1a and 1b respectively. Mass-based instruments measure parameters that are directly or computationally related to particle mass. Here, empirical inter-comparison of mass-

based instruments utilizing different measurement principles address instrument calibration and performance. The optically-based instruments measure absorption, scattering, and/or extinction of the particle ensemble at specified wavelengths. As shown in Table 1b, the optical instruments covered a wavelength range of λ = 355 nm - 1064 nm. Inter-comparisons of measurements obtained at the same wavelength provide a means for diagnosing instrument-to-instrument variability. Comparing optical measurements obtained across a range of wavelengths provides insight into the wavelength dependence of the scattering, absorption, and extinction for different types of soot particles.

Tables 1a and 1b include the name, abbreviation and manufacturer of each instrument, a brief description of the measurement provided and units for the key measured parameter. Key instruments used to characterize and continuously monitor the soot particles are listed in Table 1c. Results from instruments marked with an asterisk are not included in the present manuscript and will be presented in subsequent publications.

Table 1a. Mass-Based Instruments.

Instrument	Measurement Description	Measure	Unit
Couette Centrifugal Particle Mass Analyzer (CPMA), [Cambustion, Ltd.]	Shape-independent particle mass using centrifugal and electrostatic forces.	m_p	fg
Single Particle Soot Photometer (SP2) – 3 in number, [Droplet Measurement Technologies]	Mass of black carbon particles based on their incandescence.	m_{BC}	fg
Aerosol Mass Spectrometer (AMS), [Aerodyne Research, Inc.]	Vacuum aerodynamic diameter and mass loadings for non-refractory chemical components of submicron aerosol particles	d_{va} m_{NR}	nm μg/m^3
Scanning Mobility Particle Sizer (SMPS), [TSI]	Mobility diameter size distribution	d_m	nm
Soot Particle-Aerosol Mass Spectrometer (SP-AMS) [Aerodyne Research, Inc.]	Vacuum aerodynamic diameter and mass loadings for both non-refractory and refractory chemical components of submicron aerosol particles. Chemical ion signals obtained via intra-cavity laser vaporization (λ =1064 nm) and electron impact ionization	d_{va} $m_{R,}\, m_{NR}$	nm μg/m^3
[a]Photoelectric Aerosol Sensor for Particle-Bound Polycyclic Aromatic Hydrocarbons (PAS2000CE) [EcoChem Analytics]	Mass of surface-bound PAHs by photoionization of adsorbed PAH and measurement of the resulting positively charged particles	m_{PAH}	ng/m^3

[a]Results not included in the present manuscript and will be presented in subsequent publications.

Table 1b. Optically-Based Instruments.

Instrument	Measurement Obtained	Measure	Unit
Photoacoustic Spectrometer (PAS) [NOAA CSD]	Absorption coefficient determined from measurement of the pressure waves created by heating the particles with a modulated laser source (λ= 532nm)	β_{abs}	Mm^{-1}
Photoacoustic Soot Spectrometer (PASS-3) [Droplet Measurement Technology]	Similar to the PAS in principle, the PASS-3 measures thermal expansion at three wavelengths (λ= 405, 532, and 781 nm). The instrument is also equipped with a scattering sensor for each λ based on reciprocal nephelometry	β_{abs} β_{sca}	Mm^{-1} Mm^{-1}
Photo-Thermal Interferometer (PTI) [BNL]	Absorption coefficient of a particle based on the change in refractive index of an excited particle's proximal gases (λ = 532 nm)	β_{abs}	Mm^{-1}
Cavity Ring Down Aerosol Extinction Spectrometer (CRD-AES) [NOAA CSD]	Extinction coefficient of particles in an optical cavity (λ= 355, 532, and 1064nm) and as a function of RH	β_{ext}	Mm^{-1}
Cavity Attenuated Phase Shift Extinction Monitor (CAPS) [Aerodyne Research, Inc.]	Similar to the CRD-AES, CAPS measures extinction at (λ= 445 ± 8nm)	β_{ext}	Mm^{-1}
[a]Multi-Angle Absorption Photometer (MAAP) [ThermoElectron]	Absorption coefficient determined from the change in transmitted light (λ= 670 nm) through a filter. Corrections applied for aerosol scattering and specific	β_{abs}	Mm^{-1}

	instrument geometry		
[a]Particle Soot Absorption Photometer (PSAP) – 2 in number [Radiance Research.]	Absorption coefficients measured at λ = 470, 530 and 660nm	β_{abs}	Mm^{-1}
[a]Nephelometer [TSI]	Scattering coefficients at λ = 450 nm, 550 nm and 700 nm.	β_{sca}	Mm^{-1}

[a]Result not included in the present manuscript and will be presented in subsequent publications.

Table 1c. Particle Characterization and Monitoring Instrumentation

Instrument	Measurement Description	Measure	Unit
Condensation Particle Counter (CPC) – 3 in number [TSI]	Concentration of aerosol particles using condensation-growth and light scattering.	particles/cm^3	#/cm^3
Differential Mobility Analyzer (DMA) – 2 in number [TSI]	Size-selects the aerosol distribution by balancing electrostatic and drag forces on a charged particle distribution providing particles of known mobility diameter	d_m	nm
[a]Cloud Condensation Nuclei Counter (CCN) [Droplet Measurement Technology]	Concentration and cloud nuclei potential of aerosols. Determination of the critical supersaturation (SS_c) the supersaturation at which 50 % of the particles activate to cloud droplets	N_{CCN} SS_c	#/cm^3
[a]Diffusion Charger (DC2000CE) [EcoChem Analytics]	Active surface area of the particles in millimeters squared per cubic meter	mm^2/m^3	mm^2/m^3

	measured by diffusion charging		

[a]Results not included in the current manuscript and will be presented in subsequent publications.

The SP2 and LS-ToF-AMS mass-based instruments can provide single particle information. In this study, the CPMA and SP2 instruments report information on a mode-specific basis (i.e. particles that are singly or doubly charged in the DMA), the optically-based instruments measure ensemble average absorption, scattering, and extinction (β_{abs}, β_{sca} and β_{ext}). Because in the inter-comparison experiments discussed here, the particles are well characterized with respect to size (d_m) and concentration (particles/cm^3) per-particle absorption, scattering and extinction cross sections (σ_{abs}, σ_{sca} and σ_{ext}) can be obtained. To minimize the influence of multiply-charged particles on the measured cross-sections, all ensemble-based data shown in the manuscript have a number fraction of singly charged particles ≥ 0.93.

Coupled measurements of absorption and scattering (i.e. PASS-3) or absorption and extinction (i.e. PAS and CRD-AES) allow determination of the single scattering albedo (*SSA*) of the sampled aerosol particles. Equations 1a and b show the relationship between SSA and the measured cross-sections (σ_{sca}, σ_{abs}, σ_{ext}).

$$SSA = \sigma_{sca} / (\sigma_{sca} + \sigma_{abs}) \quad (1a)$$

$$SSA = (\sigma_{ext} - \sigma_{abs}) / \sigma_{ext} \quad (1b)$$

Single scattering albedo (SSA) values vary from near zero for black, completely absorbing aerosol particles to $SSA = 1$ for a non-absorbing aerosols.

Soot particles were produced at controlled fuel-to-air equivalence ratios in the range ~ ϕ = 2 to ϕ = 5. Experiments were conducted with (1) nascent soot particles (where the condensed organic material from the flame is present on the BC core surface, (2) nascent - denuded soot particles (primarily BC core only), (3) soot particles coated with sulfuric acid or DOS, and (4) coated and then denuded soot particles.

Of the instruments tested, the SP-AMS and CPMA are recently developed mass-based instruments and the PTI, PASS-3 and CAPS are newly developed optically-based instruments. For these instruments the present inter-comparison experiments provide the first wide-ranging operational test with fully characterized soot particles. Brief descriptions of the instruments used in the inter-comparison study are provided in the appendix.

3. Experimental Arrangement.

3.1 Particle Generation. The re-designed soot generation/sampling system is shown in Figure 1. The arrangement of the apparatus varies somewhat with specific experiments. As in our first inter-comparison study (*Slowik et al.* 2007), soot particles are produced with a McKenna flat flame burner by the combustion of a mixture of C_2H_4 (ethylene) and O_2 premixed with a dilution flow of N_2 and surrounded by a sheath flow of N_2. In the new setup, the base of the burner is mounted on an *x-y-z* translation stage and the combined soot generation/sampling apparatus is secured within a stainless steel frame attached to an optical table. This arrangement provides a stable reproducible alignment of the sampling inlet with the soot source. The figure also shows the arrangement for producing black carbon particles by atomization of aqueous suspensions.

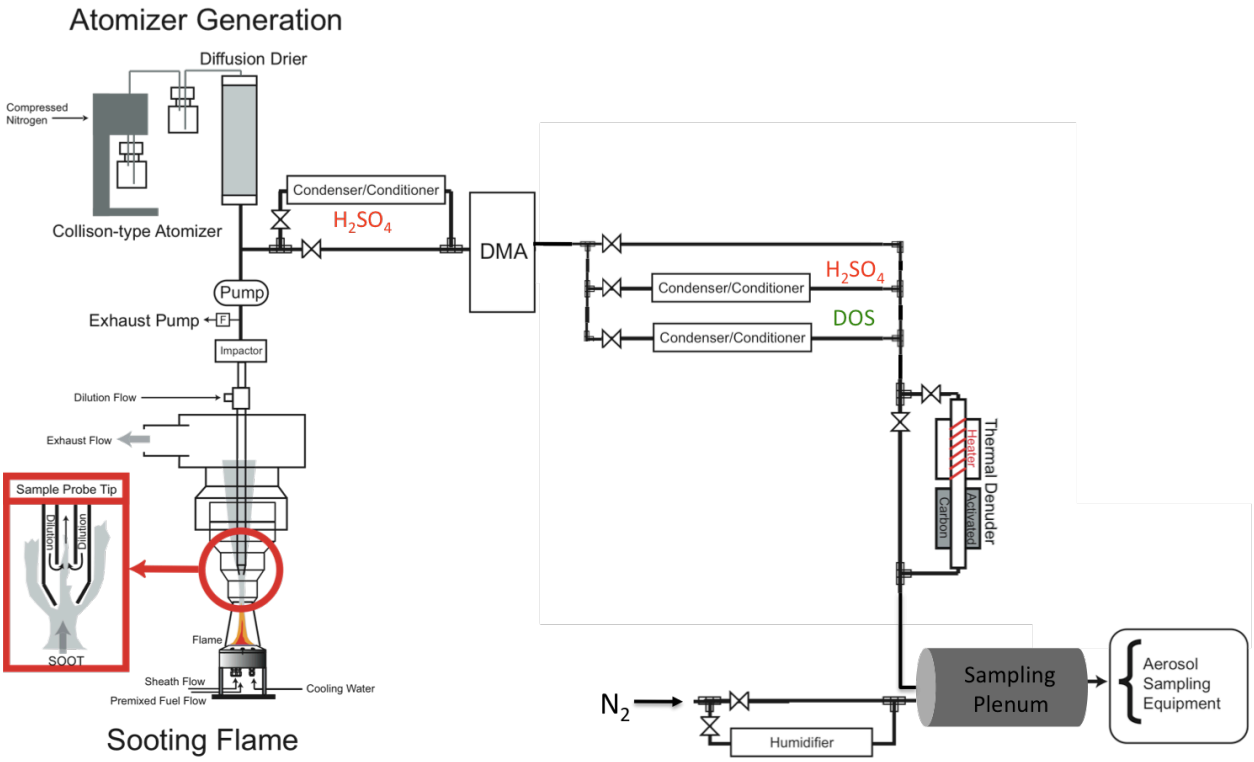

Figure 1. Particle generation/sampling apparatus

After generation, particles are size-selected with a Differential Mobility Analyzer (DMA; TSI model 3080 - calibrated and operated with a sheath flow of N_2). The improved alignment control allows the optimization of the width and peak position of the polydisperse soot distribution. As a result, the DMA can be set to select a size that corresponds to the falling edge of the polydisperse distribution thereby providing monodisperse distributions of soot particles with minimal influence from multiply charged particles. Through characterization experiments,

the optimal sampling height (distance between the burner surface and sampling inlet) was established to be ~ 8".

In Figure 2 we show examples of typical number distributions of nascent size-selected soot particles produced at a fuel equivalence ratio $\phi = 2.0 \pm 0.2$ (d_m = 31 nm, d_m = 97 nm, and d_m = 276 nm). The 1-sigma width of the d_m size distribution is approximately ± 20% controlled by the 5:1 ratio of sheath to sample flow in the DMA. Periodic monitoring of the voltage setting and flows in the DMA indicated that the mode d_m size of a typical run is stable to within 2%. The size distributions shown have less than 5% of the particle number attributed to multiply charged particles. The number fraction of singly charged particles for each experimental run was calculated from the logged SMPS number distributions and found to be in excellent agreement (within 2%) with the q1 number fraction measured with the SP2 and LS-ToF-AMS instruments. The scales for the three distributions are different as indicated by the colors.

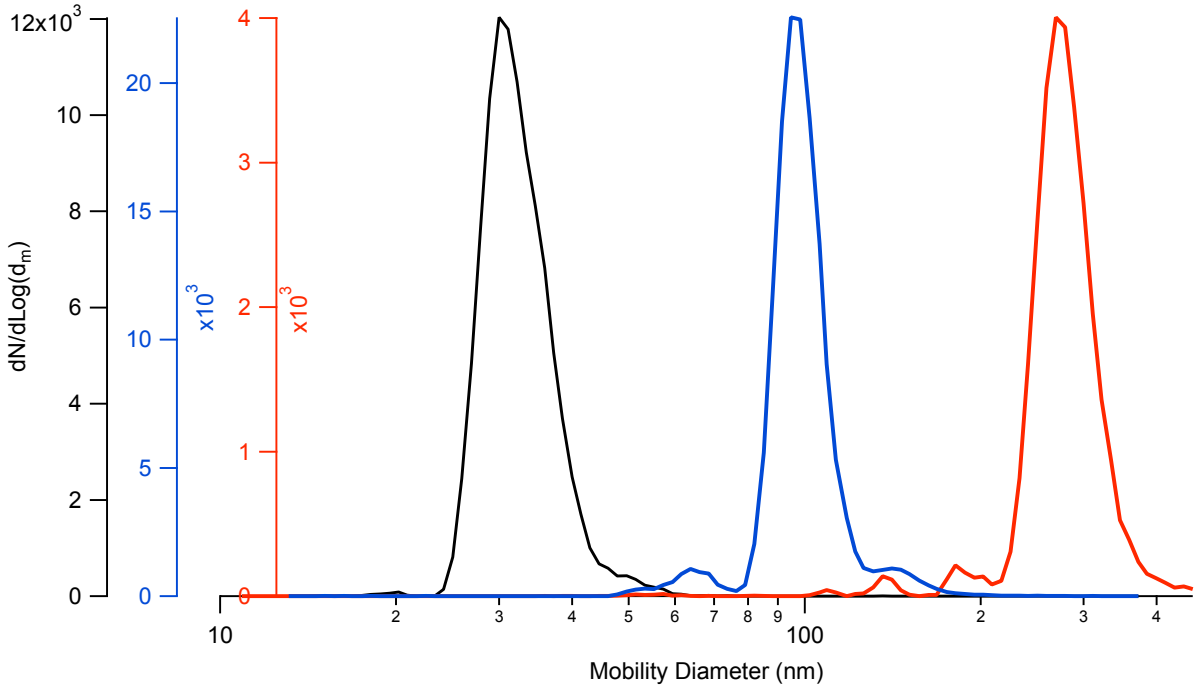

Figure 2. Three particle size distributions provided by the DMA set to size-selected mobility diameters d_m = 31 nm, d_m = 97 nm, and d_m = 276 nm obtained at a fuel equivalence ratio ϕ = 2.0 ± 0.2. The integral under each curve provides the number concentration (p/cm^3) between the limits of integration.

3.2 Flow Control and Sampling. Sensitivities of the instruments in this study vary. For accurate measurement, each instrument requires a particle number concentration in a specific range. The inter-comparison study included instruments that measure single particle properties and instruments that measured ensemble average properties. Typically, instruments that measure ensemble average properties require flows with number concentrations in the range ~ 1,000 - 50,000 p/cm^3 (dependent on particle size) while single particle instruments are most effective at concentrations of ~ 100 - 3,000 p/cm^3. Therefore, careful control of the number concentration of soot particles is essential. Flow meters, flow controllers and humidity monitors (not shown in Figure 1) were used to define, control and monitor the flows and resulting soot number concentrations throughout the inter-comparison study. All input flows to the soot source (fuel, oxygen, pre-mix nitrogen and sheath nitrogen) were carefully monitored to ensure the stability of the system for each equivalence ratio tested.

As indicated in the inset of Figure 1, a flow of N_2 (called 'dilution N_2 flow') is introduced around the sampling tip to prevent soot from clogging the inlet. The dilution N_2 flow also allows control and adjustment of the total soot particle concentration in accord with the requirements of the sampling instrumentation. By systematically varying the dilution N_2 flow in the soot-particle sampling inlet, particle number concentrations were obtained over the desired range. The

majority of the experimental runs were obtained with soot particle number concentrations between 1000-4000 particle/cm^3.

An important modification to the soot generation/sampling system was the installation of a diaphragm pump downstream of the DMA (not shown in Figure 1). The diaphragm pump is used to produce a sample flow rate of ~ 2 L/min through the DMA (~5:1 sheath: sample), keeping the size resolution of the DMA high (± 20% of the d_m mode diameter). Tests with and without the diaphragm pump integrated into the sampling line confirmed that the pump did not affect the chemical or physical properties of the soot particles across the range of d_m sizes and equivalence ratios tested in the inter-comparison study. To increase the total flow of the system to the desired 22 L/min, an additional N_2 dilution flow was incorporated into the system downstream of the DMA and the coating/denuding apparatus. This arrangement also allowed humidification of the additional N_2 flow and subsequent relative humidity (RH) control within the plenum.

After appropriate dilution and processing (if coated and/or denuded) the particles flow into the plenum chamber. From the plenum, the flows are distributed to the various instruments listed in Tables 1a, 1b, and 1c (described in greater detail in the appendix). At various points during the inter-comparison the number concentration of soot particles was monitored at each of the exit lines from the sampling plenum to confirm that no sampling biases were present.

3.3 Coating and Denuding Apparatus. In the coating and/or denuding experimental runs, the particles are passed through the requisite sections of the apparatus (See Figure 1). The coating section consists of a 36" long 3/8" diameter quartz tube with two (~12" in length) heating stages referred to as T1 and T2. Throughout the experiments, T1 was typically held ~ 30^{o}C warmer

than T2 with T1 temperatures ranging from 60-140°C, depending on the coating thickness required for each experimental condition. The coating material of interest (either DOS or H_2SO_4) was contained within a small reservoir located in the first heated section. The last 12" section of the coating tube was kept at room temperature. As shown in Figure 1, two H_2SO_4 coating reservoirs were available, one was located upstream of the DMA and a second located downstream of the DMA. The upstream reservoir was used to coat the polydisperse distribution of soot particles. In this case, coated soot particles were then size selected with the DMA. In contrast, the downstream reservoir coated size-selected soot particles.

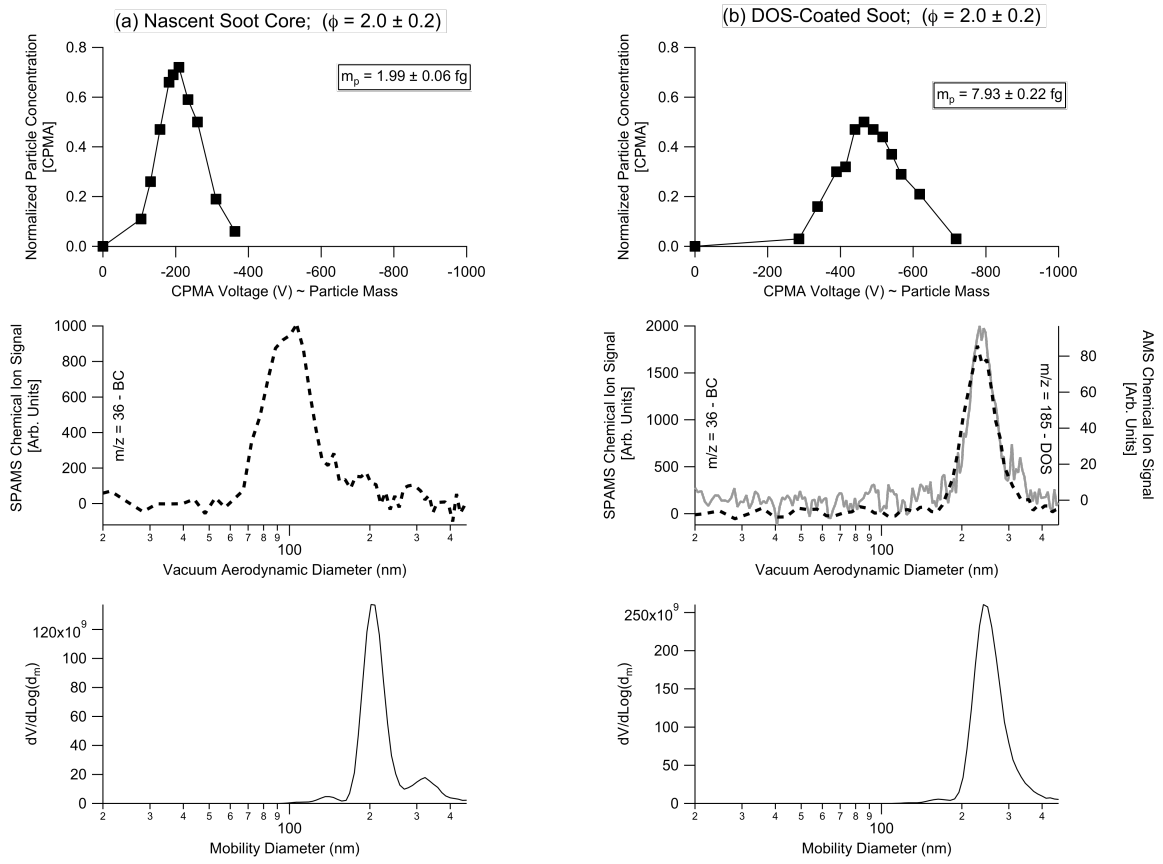

Figure 3. Measured CPMA (upper panel), vacuum aerodynamic (middle panel) and mobility (lower panel) distributions for **(a)** an uncoated nascent soot core ($\phi = 2.0 \pm 0.2$) and **(b)** the same soot core coated with DOS.

The combined information obtained with the CPMA, SP-AMS, LS-ToF-AMS, and SMPS is illustrated in Figure 3 to demonstrate measurements of both the refractory and non-refractory content of the soot particles. In Figures 3a and 3b we show the physical and chemical characterization of soot particles before and after coating with DOS. The upper panel of Figure 3 shows the normalized number concentration of the particles measured with the CPMA as a function of the CPMA voltage. The voltage obtained from the mode of a log-normal fit to the CPMA data is used to determine the particle mass. The CPMA sample flow rate was held constant at 0.3 L/min during the experiments and the rotational speed was varied with particle size to maintain optimal mass resolution across the range of conditions studied. Specifically, λ_{CPMA}, a dimensionless number that quantifies the CPMA mass resolution was kept within a range from $-0.3 \leq \lambda_{CPMA} \leq -0.1$ (See Eq. 13 in *Olfert and Collings*, 2005). The middle panel shows the measured chemical ion signals as a function of their measured vacuum aerodynamic diameter. For the nascent soot core, the chemical ion signals for m/z = 36 (refractory BC signal) measured with the SP-AMS is shown. For the DOS-coated condition, the m/z 36 (from the SP-AMS) and m/z 185 (non-refractory organic signature of DOS measured with the LS-ToF-AMS) are shown. The bottom panel of the figure shows the volume distributions measured with the SMPS instrument showing the change in mobility diameter as a result of the DOS coating.

The thermal denuder, designed and characterized by Aerodyne Research Inc. in collaboration with the University of Colorado (*Huffman et al.* 2008) consists of a 22" heated section held at 250^{o}C followed by a 24" section of activated charcoal kept at room temperature.

As particles pass through the heated region, the non-refractory components on the particles vaporize and are then adsorbed by the activated charcoal. As a result, for this study, the operational definition of "non-refractory material" is matter that is removed from the particles at 250^{o}C in the denuder. Likewise, refractory material is that which remains in the particle phase after passing through the denuder. Experimentally, the particles transmitted through the denuder are the black carbon cores generated under the specific experimental condition. The composition of the denuded soot particles was confirmed with the LS-ToF-AMS by the absence of measurable chemical ion signals due to non-refractory material during denuded particle runs. The denuder was used to systematically examine the size (d_m, d_{va}), mass-mobility exponent (D_{fm}), and mass of the BC core for each condition tested: Nascent soot ($2.0 \leq \phi \leq 5.0$), DOS-coated soot ($\phi = 2.0 \pm 0.2$), and H_2SO_4-coated soot ($\phi = 2.0 \pm 0.2$). That is, for a given 'coated' experimental run, there is a corresponding denuded experimental run.

4. Experimental Objectives and Selected Results for Mass-Based Instruments.

4.1 Couette Centrifugal Particle Mass Analyzer (CPMA).

In conjunction with the DMA and CPC instruments, the CPMA provides the most direct, shape-independent measure of particle mass (Olfert and Collings, 2005). To illustrate the utility of the CPMA measurements we **(a)** validated the calibration of the CPMA with polystyrene latex spheres (PSL) of known diameter and density, **(b)** used the CPMA-measured mass (m_p) of nascent and denuded soot runs to determine the mass fraction of black carbon in soot particles produced at different equivalence ratios, **(c)** used the CPMA-measured mass in conjunction with

the known d_m to determine the mass-mobility exponent of soot particles produced at different fuel equivalence ratios, and **(d)** monitor changes in the morphology coated and denuded soot particles.

4.1a Calibration. In Figure 4 we show the CPMA-determined particle mass for commercially manufactured PSL particles (Duke Scientific, Corp.) as a function of the calculated mass (based on the known density $\rho = 1.054$ g/cm^3 and diameter (d_p) of the PSL particles.

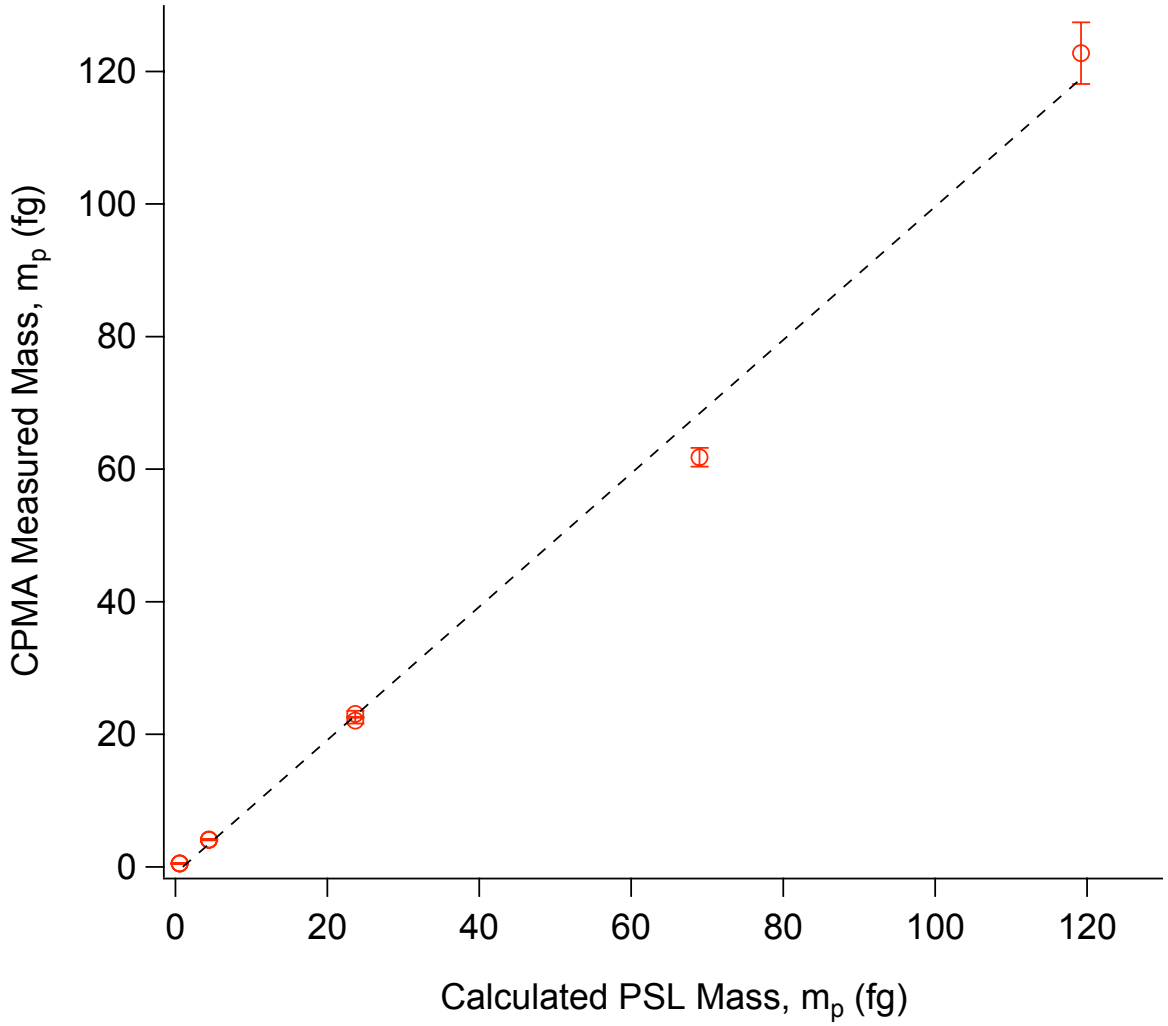

Figure 4. CPMA-measured mass for commercially manufactured PSL particles as a function of calculated particle mass (via density and size). Linear regression fit to the data yields a slope of 1.01 and $R^2 = 0.998$.

The CPMA-measured PSL particle mass is in good agreement with the calculated PSL mass across a mass range of m_p = 0.1-120 fg. The error bars shown in the CPMA measured mass axis correspond to the 1-sigma width of the log-normal fit to the mass distribution obtained with the CPMA.

4.1b Black carbon mass content of soot particles. During the inter-comparison studies, experimental runs with nascent and/or coated soot particles were coupled with corresponding denuded soot runs. In this way, the size, shape and mass of the refractory BC core were characterized after the condensed phase organic or inorganic material was removed.

With the CPMA measurement, nascent soot runs coupled with corresponding denuded runs provide a measure of the mass fraction of BC in the nascent soot produced at different fuel equivalence ratios (ϕ). Figure 5 displays the CPMA-measured mass for nascent soot (y axis) versus the CPMA-measured mass for the corresponding denuded soot particles. Measurements shown in the figure were obtained for soot particles produced at equivalence ratio of $\phi = 2.0 \pm 0.2$ (red crosses) and $\phi = 5.0 \pm 0.2$ (black circles). The range of mass values displayed was obtained by varying the mobility size (d_m) of the particles.

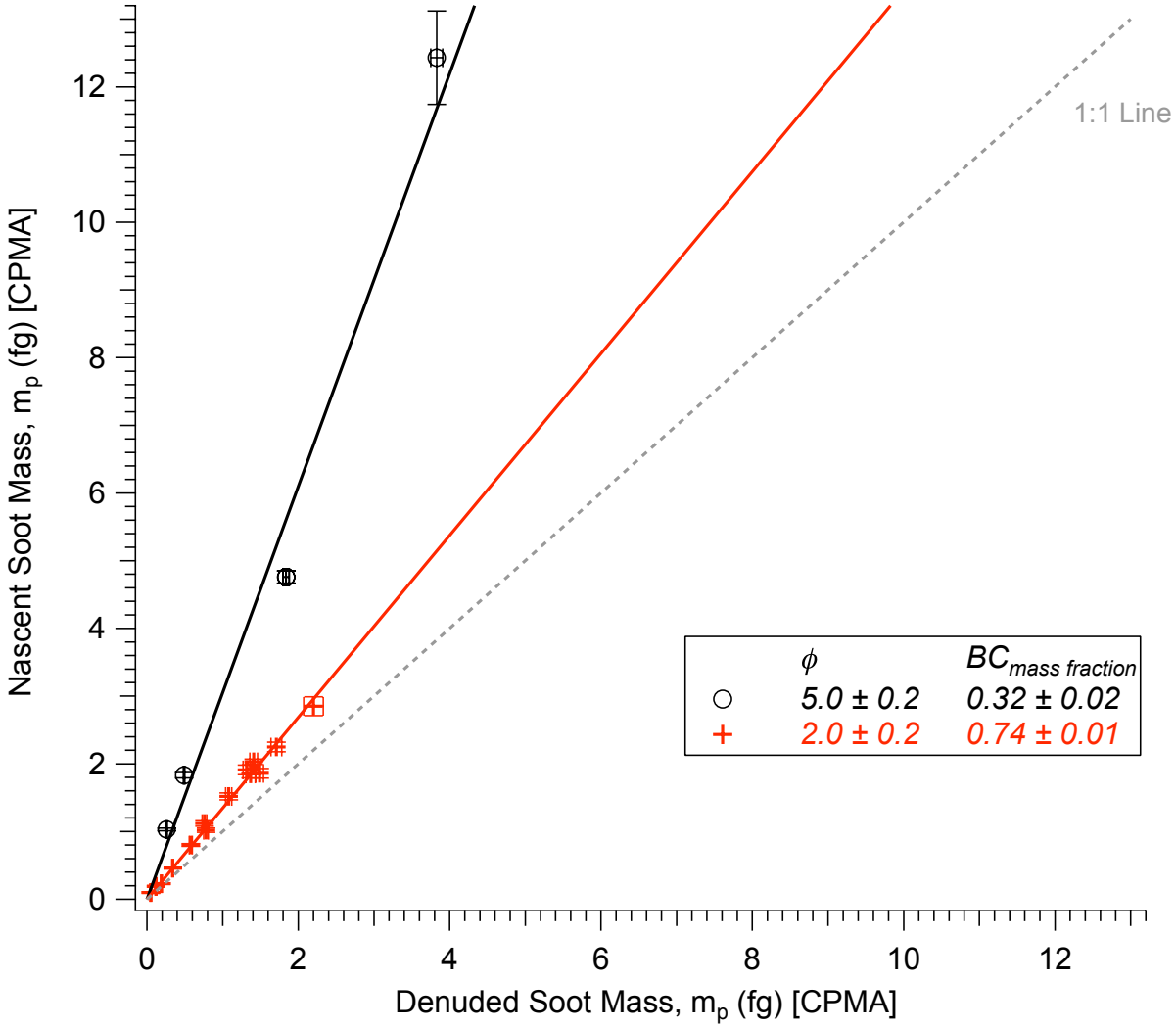

Figure 5. CPMA-measured mass for nascent soot particles (*y*-axis) plotted as a function of the CPMA-measured mass for the corresponding denuded soot particles (*x*-axis). That is, soot particles having the same refractory core are compared before and after denuding. The error bars shown correspond to the 1σ standard deviation in the CPMA mass measurement.

The results in Figure 5 show that the BC mass fraction of soot particles produced at ϕ = 2.0 ± 0.2 is on average 0.74 while soot produced at ϕ = 5.0 ± 0.2 has a BC mass fraction of 0.32. The lower BC mass fraction of soot particles produced at the high (*i.e.* fuel rich) equivalence ratios is consistent with incomplete combustion producing more condensable organics (aliphatic and PAH) within the flame that subsequently coat the refractory BC core.

4.1c Measurement of particle mass-mobility exponent. The mass-mobility exponent (D_{fm}) is obtained from the relationship between the measured mass (m_p) and mobility diameter (d_m) via equation 2 (*Park et al.* 2004):

$$m_p = C' d_m^{Dfm} \qquad (2)$$

where C' is a proportionality constant and D_{fm} yields the power law dependence between the particle mass and the hydrodynamic length scale. The mass-mobility exponent (commonly referred to as the 'mass fractal dimension') is an estimate of the fractal dimension (D_f). Fractal dimensions can also be estimated from light scattering (*Wang and Sorensen,* 1999) or microscopy measurements (*Koylu et al.* 1995; *Park et al.* 2004). Each approach to estimating fractal dimension (mass-mobility, light scattering, and microscopy) has its own set of underlying assumptions. Therefore, it is important to identify how the specific technique used is related to the fractal dimension.

Equation 3 shows how D_f is related to the soot particle properties as described by Hinds (1999):

$$N_{pp} = C \cdot (2R_g/d_{pp})^{Df} \qquad (3)$$

Here, N_{pp} and d_{pp} are the number and diameter of the primary spherules comprising the aggregate, C is a proportionality constant, and R_g is the radius of gyration. If one assumes that d_{pp} is constant for soot particles produced at a given equivalence ratio, then R_g is proportional to d_m and N_{pp} is linearly proportional to the particle mass. Equation 3 then simplifies to equation 2 and measurements of d_m and m_p yield the factor D_{fm}. It has been shown that R_g is proportional to d_m for soot particles with $D_f > 2$ (*Schmidt-Ott et al.* 1990).

For the results presented here, the CPMA provides a direct measure of m_p, and for a given series of experimental runs over which d_m was varied and the soot particle type (i.e. equivalence ratio) was held constant, D_{fm} can be determined. Figure 6 shows a plot of the CPMA-measured mass as a function of the selected d_m for nascent soot particles produced at $\phi = 2.0 \pm 0.2$ (red open symbols) and $\phi = 5.0 \pm 0.2$ (black solid circles). The dashed lines in the figure are linear fits to the data and indicate that nascent soot produced at $\phi = 2.0 \pm 0.2$ has a $D_{fm} = 2.24 \pm 0.03$ (fractal aggregate) whereas the nascent soot produced at $\phi = 5.0 \pm 0.2$ has a $D_{fm} = 3.04 \pm 0.04$ (near-spherical). This observation is consistent with the significantly larger non-BC mass fraction (~ 0.74) of the $\phi = 5.0$ soot particles compared to the $\phi = 2.0$ soot particles shown in Figure 5. We note that the mass-mobility exponents reported here represent the ensemble average D_{fm} for each type of soot particle produced.

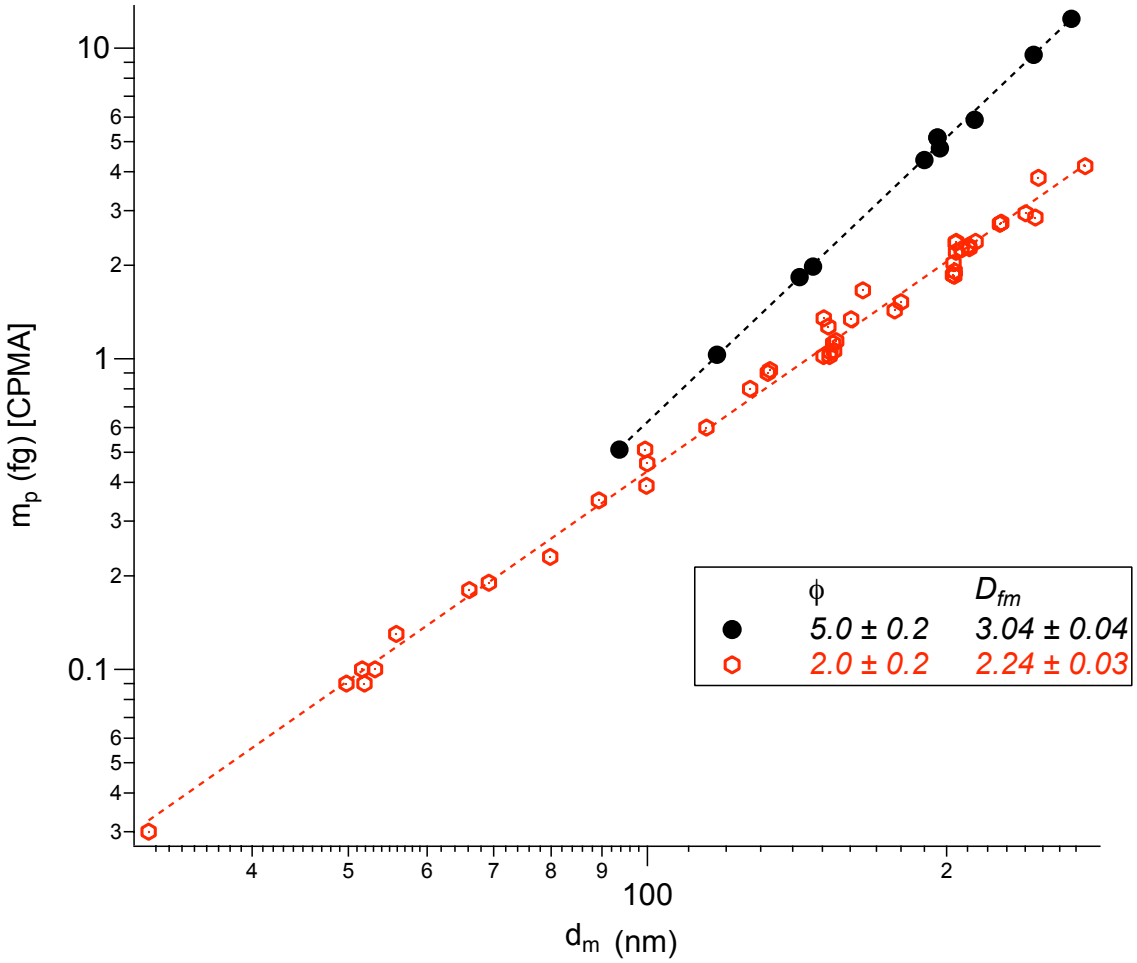

Figure 6. CPMA-measured particle mass for nascent soot particles produced at ϕ = 2.0 ± 0.2 and ϕ = 5.0 ± 0.2 as a function of mobility diameter. Fits shown as the dashed lines indicate that the low equivalence ratio soot particles are fractal-like with a D_{fm} = 2.24 ± 0.03 whereas the high equivalence ratio soot particles are near-spherical with a D_{fm} = 3.04 ± 0.04.

As is evident in Figure 6, the two linear fits shown do not have the same intercept (C') value and appear to cross at d_m ~ 60 nm. This phenomenon is the result of differences between N_{pp} > 60 vs. N_{pp}< 60 regimes (*DeCarlo et. al.* 2004). The fractal dimension (or mass-mobility

exponent) is higher for N_{pp}< 60. This is obvious for the extreme case; for a particle with N_{pp} =1, D_{fm} = 3. Likewise, an aggregate of 2 spherules must have the most compact possible shape. However, as more spherules are added, the length scale grows more rapidly with respect to N_{pp}, eventually approaching the N_{pp} >~60 limit. In other words, soot particles are not true fractals in the mathematical sense: their self-similarity does not hold across infinite length scales, and breaks down in the limit of small N_{pp}.

Within experimental uncertainties, the relationship between log(m_p) and log(d_m) is well described by a linear fit. Size-dependent changes in either C' or D_{fm} would be expected to appear as a change in slope of the line, which is not observed for the size range studied. From this observation, we conclude that within uncertainties in our measurements, the data are well represented by a size-independent D_{fm} value.

4.1d Effect of coating-denuding process on soot particle re-arrangement. To explore whether the fractal soot particles undergo re-arrangement as a result of the coating-denuding process we measured the mass-mobility exponent of the particles at each stage of the coating-denuding process. In Figure 7a we show the plot of m_p versus d_m for DOS-coated and DOS-coated-denuded soot particles produced at $\phi = 2.0 \pm 0.2$. In Figure 7b we show a similar plot for H_2SO_4-coated and H_2SO_4-coated-denuded particles. The dashed line shown in each plot represents the mass-mobility relationship for nascent-denuded $\phi = 2.0 \pm 0.2$ soot particles that have not been coated with either DOS or H_2SO_4. The slope of the dashed line (D_{fm} = 2.12 ± 0.04) represents the mass-mobility exponent of nascent-denuded soot particles produced at ϕ = 2.0 ± 0.2.

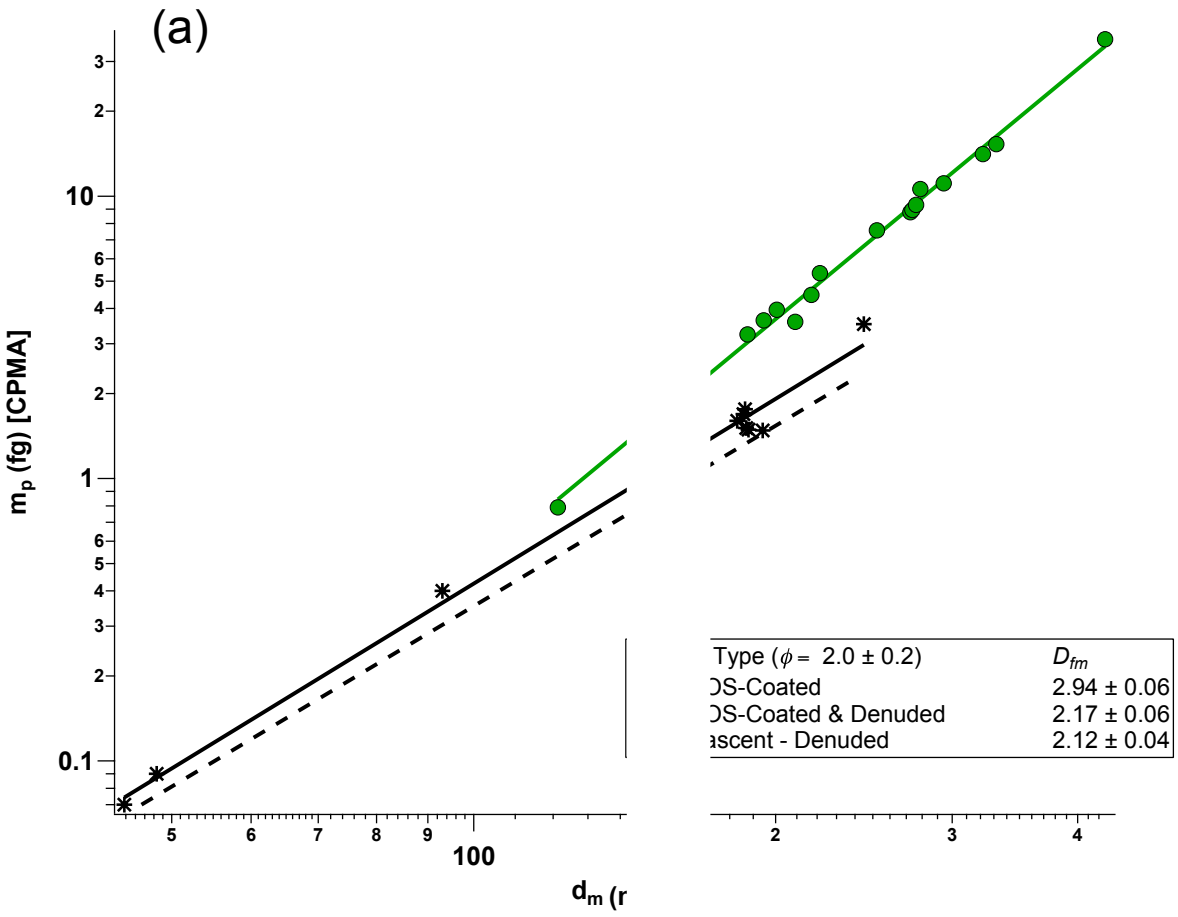
(a)
m_p (fg) [CPMA]
d_m (r
Type (ϕ = 2.0 ± 0.2)
D_{fm}
OS-Coated
2.94 ± 0.06
OS-Coated & Denuded
2.17 ± 0.06
ascent - Denuded
2.12 ± 0.04

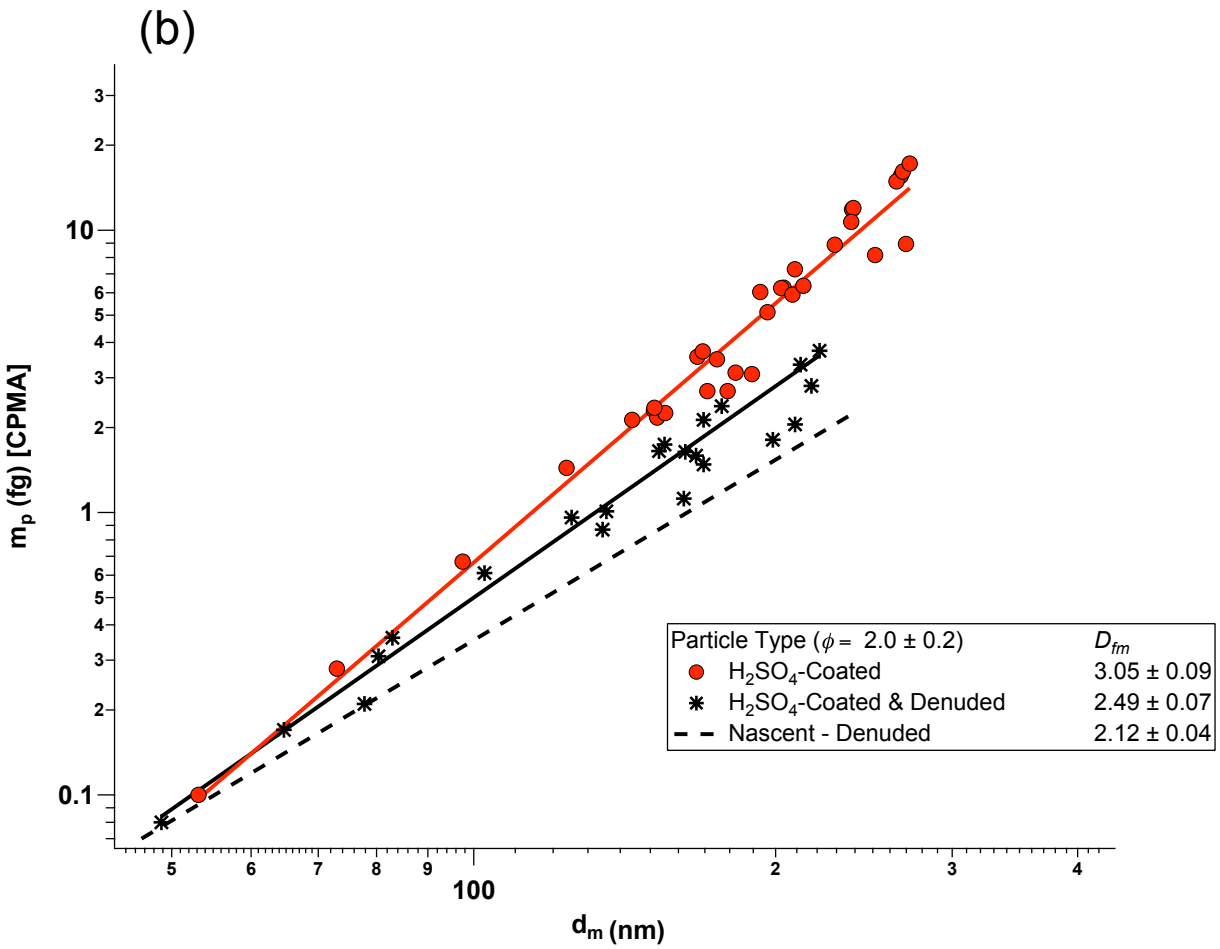

Figure 7. CPMA-measured m_p as a function of the d_m for (a) DOS-coated & DOS-coated-denuded soot runs and (b) H_2SO_4-coated & H_2SO_4-coated-denuded soot runs. In all runs shown, original soot cores were produced at $\phi = 2.0 \pm 0.2$. For reference, the dashed line in each plot shows the $D_{fm} = 2.12 \pm 0.04$ measured for nascent-denuded soot particles.

The coating mass fractions ranged from ~ 0.40 – 0.99 for the data shown in Figures 7a and 7b. The data show, that across this range of coating mass fractions, the coated soot particles (either DOS or H_2SO_4) have a D_{fm} ~ 3 (near-spherical). The DOS-coated-denuded soot particles

shown in Figure 7a retain their fractal aggregate shape with a measured D_{fm} = 2.17 ± 0.06. However, the H_2SO_4-coated-denuded soot particles, shown in Figure 7b, have a D_{fm} = 2.49 ± 0.08 indicating that the H_2SO_4-coating-denuding process has caused the soot particles to undergo re-arrangement toward a more compact shape (from D_{fm} = 2.12 to D_{fm} = 2.49).

A pictorial view of the coating-denuding process is displayed with sample SEM images shown in Figure 8. The figure includes an SEM image for **(a)** a nascent soot particle; **(b)** a DOS-coated-denuded soot particle, and **(c)** a H_2SO_4-coated-denuded soot particle. In all three cases the original soot particles were generated at ϕ = 2.0 ± 0.2 and size selected at d_m = 209 nm. The large black regions are holes in the SEM filter surface to allow sufficient gas flow for impaction. These images are consistent with the data displayed Figures 7a and 7b. The H_2SO_4 coating causes the fractal soot core to collapse to a more compact shape whereas the DOS coating does not appear to influence nearly as strongly the fractal nature of the original soot core. The observation of soot particle collapse as a result of the H_2SO_4-coating-denuding process is consistent with the observations of Zhang et al. (2008) and Pagels et al. (2009) who measured soot particle collapse after coating with H_2SO_4 with Transmission Electron Microscopy (TEM) in conjunction with DMA-APM techniques. Previous work by Kutz and Schmidt-Ott (1992) has suggested that the driving force for agglomerate rearrangement is the surface tension force of the condensed material on the soot core. The surface tension of DOS is much smaller than that of H_2SO_4. The suggested surface tension mechanism is a possible explanation for the observed difference in the H_2SO_4 and DOS rearrangement.

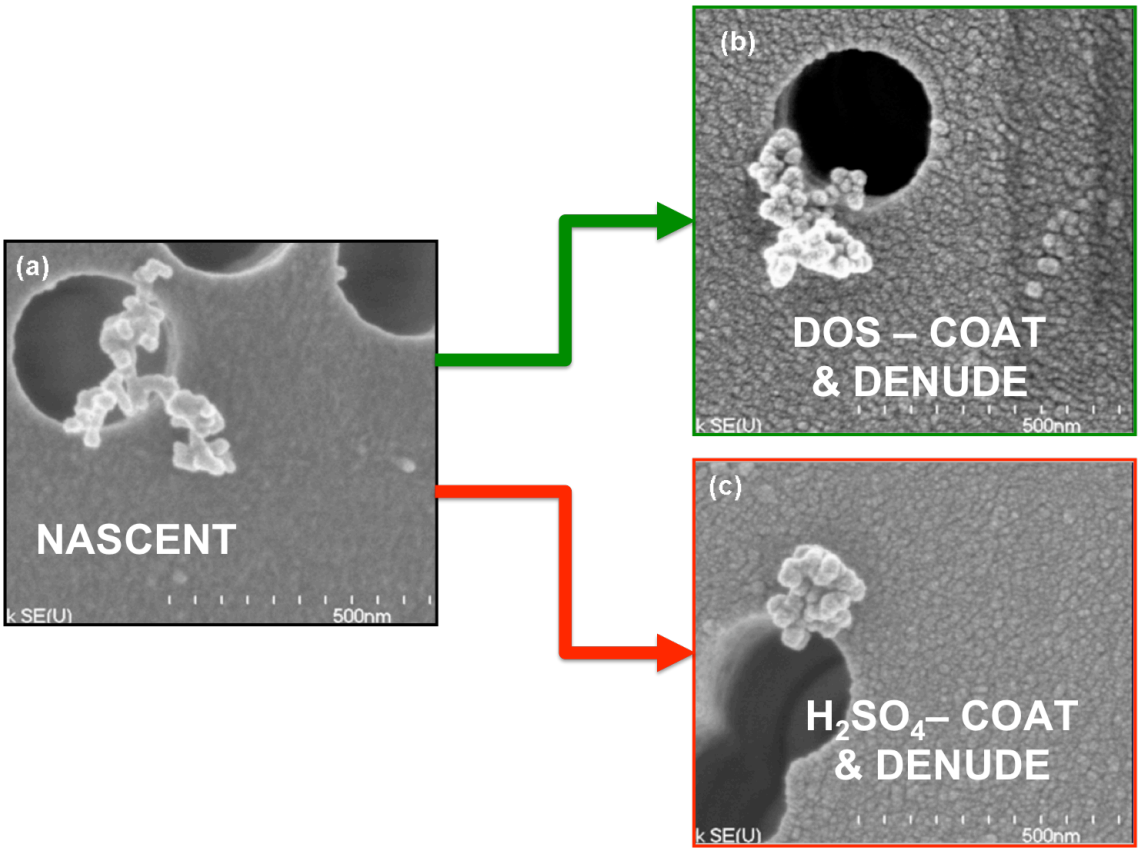

Figure 8. SEM images showing the effect of the coating/denuding process for fractal soot particles generated at ϕ = 2.0 ± 0.2 with an original mobility diameter of d_m = 209 nm; **(a)** nascent soot particle; **(b)** DOS-coated then denuded soot particle, and **(c)** H_2SO_4-coated then denuded soot particle. The dark circles are holes that are part of the particle collecting polycarbonate membrane. The images were collected using a Hitachi S-4700 field emission scanning electron. Before imaging, the filters were coated with platinum. The visible granularity of the background in some of the images is due to coating.

4.2 Comparison of CPMA and AMS-SMPS Instruments.

Both the CPMA and AMS-SMPS instruments provide particle mass determination for size selected aerosol particles. There is however an important difference between the data provided by the two instruments. The CPMA yields the total per-particle mass and does not provide a separate evaluation of the black carbon mass in the particle. (Recall that the data shown in Figure 5 are obtained in two separate sequential runs: nascent, then denuded.) The AMS instrument directly measures the non-refractory mass of the particles (i.e. chemical components that readily vaporize at temperatures of 600^{o}C and ~10^{-7} torr). The combination of the AMS and SMPS measurements provides a means for determining the refractory (i.e. black carbon) mass in the same particle, via a system of equations described in DeCarlo et al. (2004) and Slowik et al. (2004). The objective of this section is to inter-compare the CPMA and AMS-SMPS mass measurements.

Figure 9 plots the per-particle mass obtained via the AMS-SMPS measurements as a function of the CPMA-measured particle mass for (a) nascent soot generated at $\phi = 5.0 \pm 0.2$, (b) nascent soot generated at $\phi = 2.0 \pm 0.2$, (c) DOS-coated soot ($\phi = 2.0 \pm 0.2$), and (d) H_2SO_4-coated soot ($\phi = 2.0 \pm 0.2$). The AMS-SMPS mass measurements were obtained using the measured d_{va}, d_m, and non-refractory composition of the particles as discussed in DeCarlo et al. (2004) and Slowik et al. (2004).

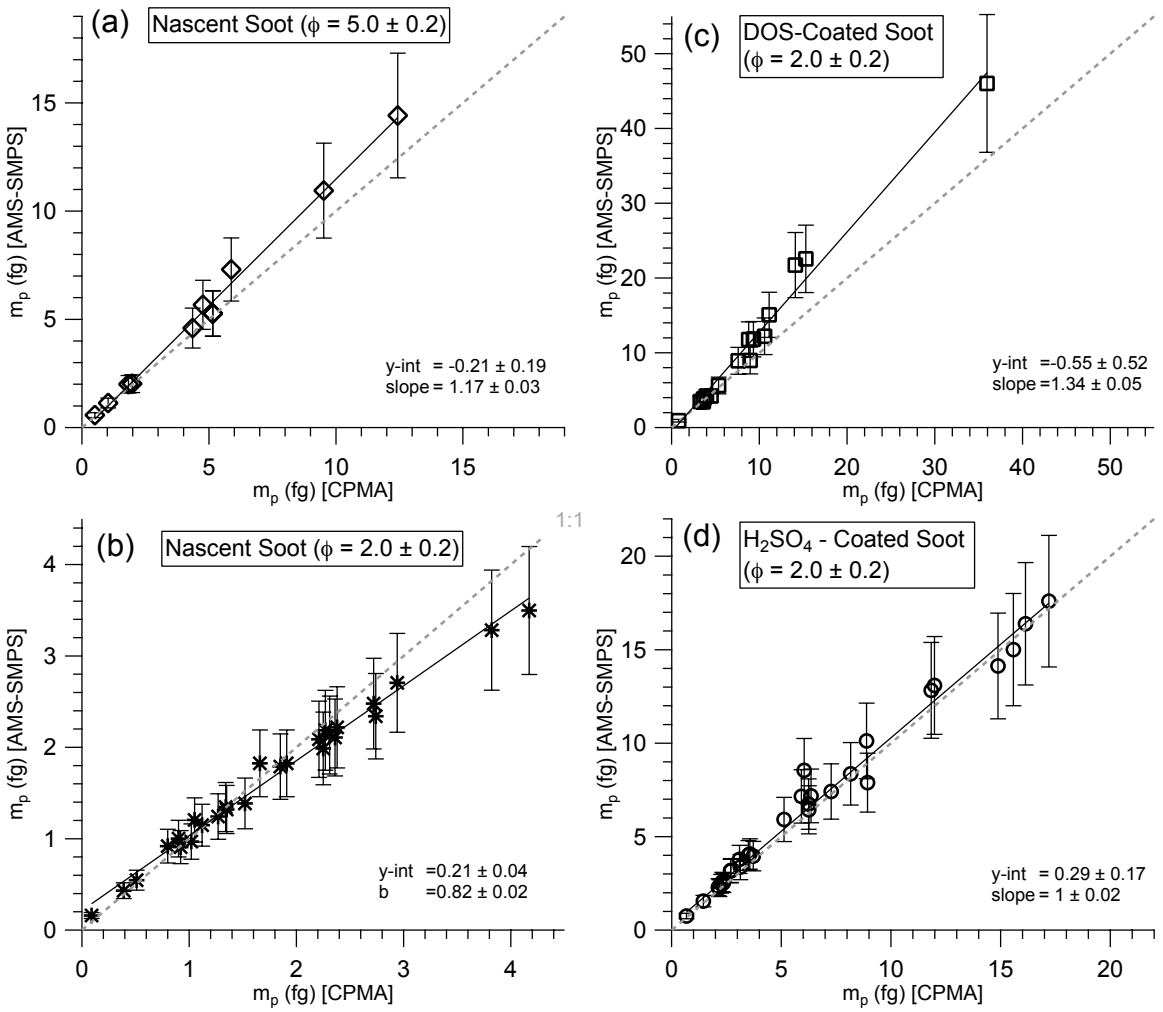

Figure 9. Per-particle mass obtained via the AMS-SMPS measurements versus the CPMA-measured particle mass for (a) nascent soot generated at $\phi = 5.0 \pm 0.2$, (b) nascent soot generated at $\phi = 2.0 \pm 0.2$, (c) DOS-coated soot ($\phi = 2.0 \pm 0.2$), and (d) H_2SO_4-coated soot ($\phi = 2.0 \pm 0.2$). The slope and intercept of linear fits to the data are shown in each panel. The 1:1 line is shown as the dashed line in each plot. Note that the different axes in each panel, a consequence of the different mass ranges obtained for each particle type studied.

As was stated, the BC mass provided with the AMS-SMPS instrument is not directly measured, rather the mass is calculated via a system of equations based on the measured d_{va}, d_m and non-refractory composition of the particles (*Slowik et al.* 2004). The overall uncertainty of the AMS-SMPS method for mass determination is principally governed by the uncertainty of the d_{va} and d_m measurements. For this experiment, the uncertainty in the AMS-SMPS mass is estimated to be ± 20%. For the H_2SO_4-coated soot particles, the two mass measurements are in agreement. For the heavily coated soot particles (ϕ = 5.0 ± 0.2 (~ 0.74 non-refractory mass fraction) and DOS-coated (0.10-0.99 organic mass fraction), the SMPS-AMS measurements are ~17% and 30% higher than the CPMA measurements. For the nascent soot particles produced at ϕ = 2.0 ± 0.2, the SMPS-AMS mass measurements is ~18% lower than the corresponding CPMA measurements. Overall, we consider the agreement between these two independent measurements of mass to be reasonable.

4.3 Performance of the SP2 Instruments.

Three Single Particle Soot Photometer (SP2) instruments were tested in these studies. The instruments were from the University of Hawaii (UH), Droplet Measurement Technologies (DMT) and the National Oceanic and Atmospheric Administration Chemical Sciences Division (NOAA, CSD). The experiments with the SP2 instruments had the following goals: **(a)** Measure, inter-compare and calibrate the incandescence signals obtained from the three SP2 instruments as a function of black carbon particle mass, **(b)** Determine the effect of particle shape on the SP2 measurement of BC mass, **(c)** Investigate how DOS and H_2SO_4 coatings affect the SP2 measurement of BC mass**, (d)** Determine the lower limit for BC mass detection in the

SP2 and **(e)** Determine SP2 response for several types of atomized carbonaceous materials – this latter aspect of instrument performance (item 'e') will be discussed in a separate publication.

4.3a Inter-comparison and calibration of the incandescence SP2 signals. The nomenclature associated with the various forms of carbon-containing aerosol at varying levels of purity is generally vague and complex. The SP2, through its detection scheme, measures only the mass of refractory material capable of reaching temperatures of ~ 4000K without vaporizing. We refer to the SP2 determination here, then, as being appropriate for "refractory black carbon" (rBC), as discussed in deeper detail in Schwarz et al. (Submitted to AS&T, 2010). In the measurements of carbon-containing combustion aerosol here and in the atmosphere this material is believed to be equivalent to "black carbon" as used in measurements of optical absorption, and most refractory components of EC identified by thermal decomposition analysis.

Figure 10 displays the incandescence signal for the three SP2 instruments as a function of total per-particle mass measured by the CPMA instrument for denuded soot particles produced at $\phi = 2.0 \pm 0.2$. Three different types of denuded particle are displayed in the figure: (1) nascent-denuded (2) DOS-coated and denuded, and (3) H_2SO_4-coated and denuded. Because the soot particles are denuded they are primarily composed of black carbon. Therefore, for the denuded subset of experimental runs, the CPMA-measured particle mass is also the BC mass. As can be seen in Figure 10, SP2 response is a linear function of the BC mass of the particles. The linear fit (using all denuded particle types) for each SP2 instrument provides a per-particle incandescence-to-BC mass calibration for the individual SP2 instruments.

While the absolute magnitudes of the incandescence signals for the three instruments differ due to differences in the operating conditions and settings of each SP2, each calibration curve fits a straight line correlation with $R^2 = 0.98$.

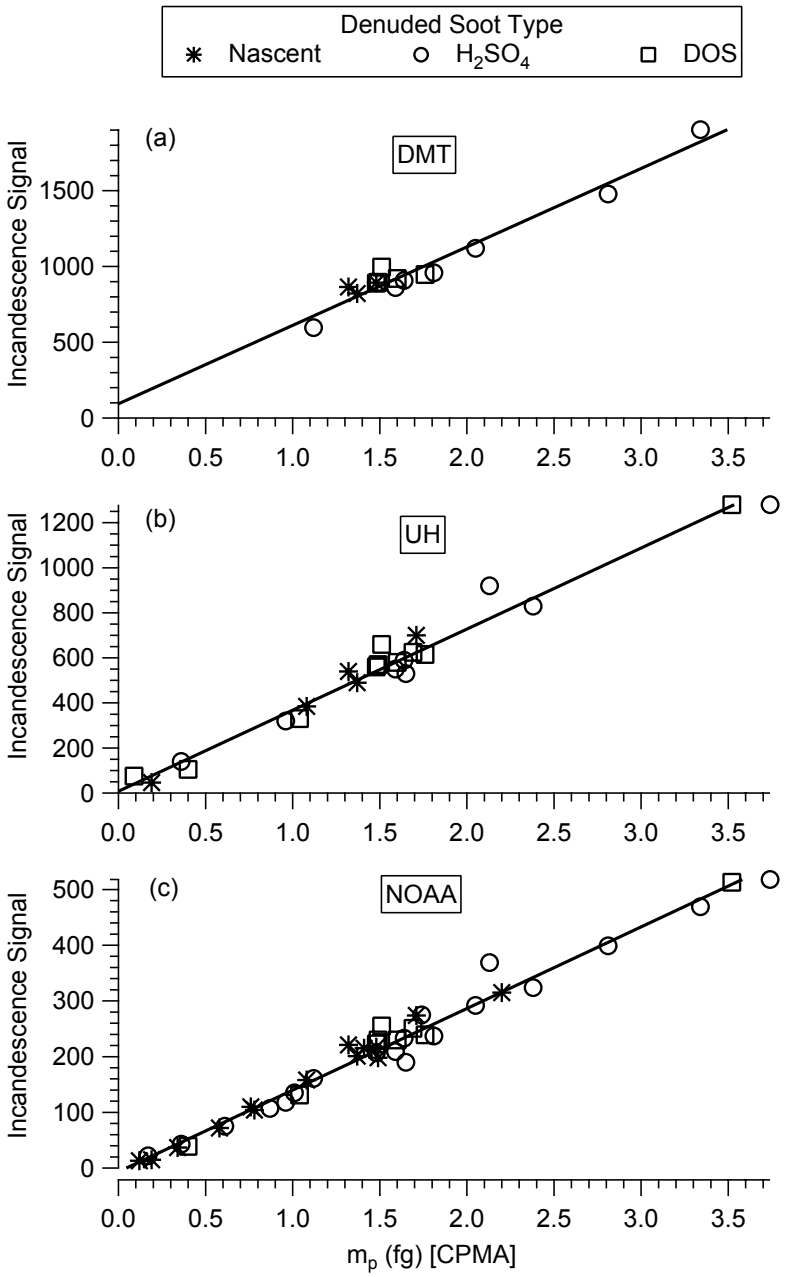

Figure 10. Incandescence signal for the three SP2 instruments plotted versus the CPMA-measured mass. Experiments were performed with denuded soot particles produced at $\phi = 2.0 \pm 0.2$. Three different denuded particle types are shown: (1) nascent-denuded (stars) (2) DOS-coated-denuded (open squares), and (3) H_2SO_4-coated-denuded (open circles). Denuded soot particles are primarily composed of black carbon. Therefore, the CPMA-measured particle mass

is also the BC mass and each plot provides an empirical incandescence mass calibration for the specific SP2 instrument. The R^2 value for the linear fits is 0.98 for all three instruments. Linear fits are based on the instrument response to all three denuded particle types. The different slopes between the three instruments merely represent three choices of operational gain for the detectors.

4.3b Effect of particle shape on SP2 measurements. Given the different types of denuded particles displayed in Figure 10, it is possible to examine the influence of BC particle shape on the SP2 incandescence signal. Recall from Figures 7 and 8 that the H_2SO_4-coated-denuded particles undergo re-arrangement resulting in a partially collapsed, more compact BC core. This is in contrast to the nascent-denuded and DOS-coated-denuded particles, which retain their fractal shape. The data in Figure 10 show no measurable difference in SP2 incandescence between the collapsed (H_2SO_4-coated-denuded) and fractal (nascent or DOS-coated-denuded) soot. This result indicates that SP2 incandescence is independent of particle shape within the range of denuded morphologies and particle sizes tested during the inter-comparison ($2.10 < D_{fm} < 2.5$).

4.3c Effect of coatings on SP2 measurements. To determine the influence of coatings (condensed organics from the flame, DOS, or H_2SO_4) on the SP2 instrument response we plot in Figure 11 the SP2-measured incandescent mass for coated soot particles as a function of the SP2-measured incandescent mass for the corresponding denuded particles (with the coating material removed). Data shown in the figure were obtained with the NOAA SP2 instrument. Similar results were obtained with the UH and DMT SP2 instruments. The format of Figure 11 is similar

to Figure 5 that presented the CPMA-measured mass for correlated nascent and denuded soot runs. Here, the SP2 measurement of BC can be directly compared in the presence and absence of substantial amounts of non-absorbing coatings.

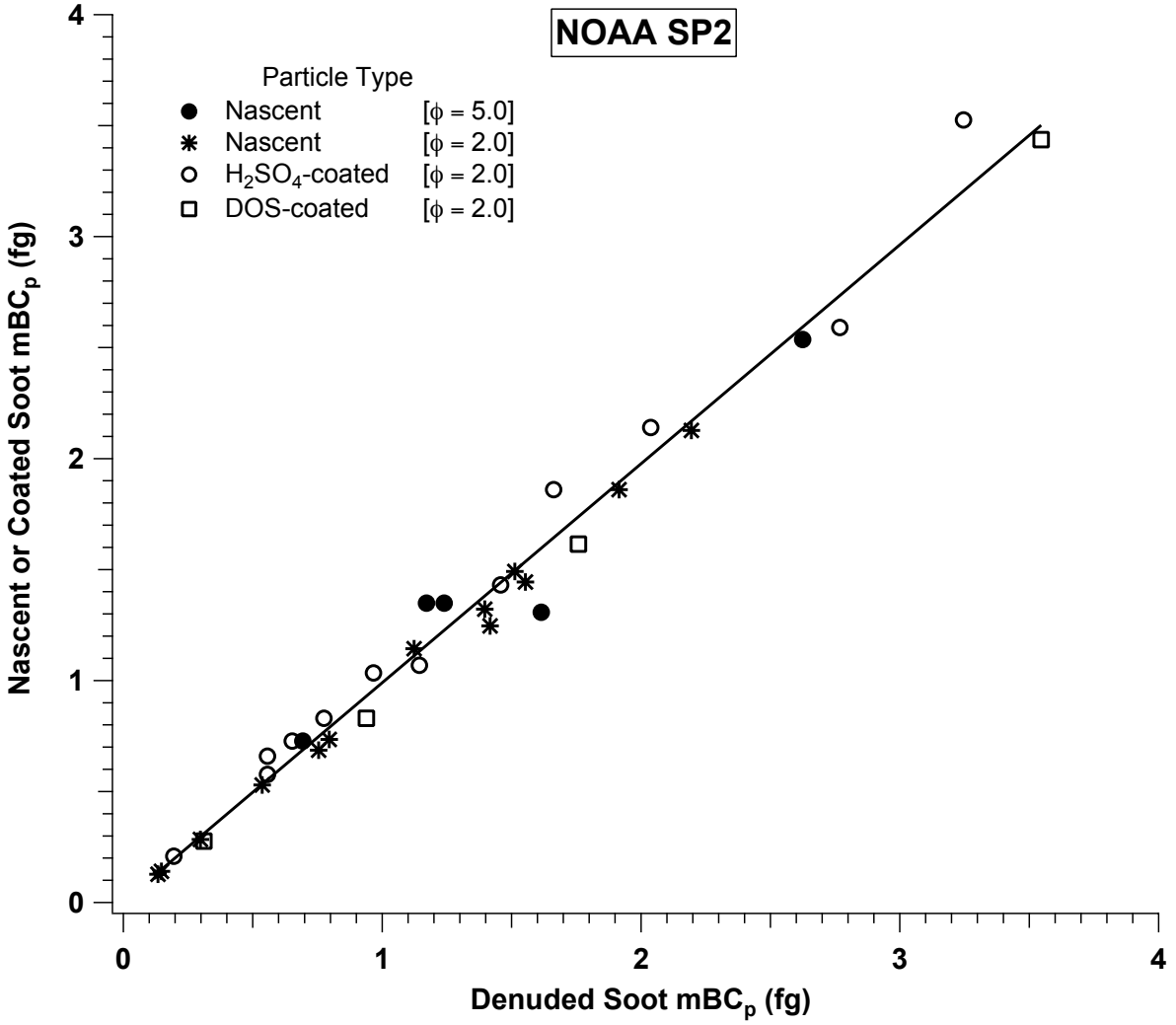

Figure 11. SP2-measured BC mass (mBC_p) for coated soot particles: nascent $\phi = 5.0 \pm 0.2$, nascent $\phi = 2.0 \pm 0.2$, DOS-coated $\phi = 2.0 \pm 0.2$, and H_2SO_4 -coated $\phi = 2.0 \pm 0.2$ plotted as a function of the SP2-measured mBC_p for the corresponding denuded soot particles. Slope of a linear fit to the data (shown as the solid line) is 0.99 ± 0.02 with a $R^2 = 0.99$.

A linear fit through the data points in Figure 11 (solid line) has a slope of 0.99 and R^2 = 0.99. This result indicates that across the range of coating types and thicknesses studied during the inter-comparison the SP2 determination of black carbon mass remained accurate. These observations are consistent with the results obtained for oleic acid and anthracene coatings in the first inter-comparison study (*Slowik et al.* 2007a).

4.3d Lower detection limit for measurement of BC mass in soot particles. One of the objectives of the inter-comparison study was to determine the detection limit of the SP2 instrument when operated under typical SP2 laser intensity settings. The specifics of such determinations are discussed in Schwarz et al. (2010). Here we simply note that, based on the results from the inter-comparison project, the SP2 instrument (under typical operating conditions) can reliably measure absorbing particles with volume-equivalent diameter (d_{ve}) ≥ 90 nm (BC mass of ~ 0.7 fg).

5. Experimental Objectives and Selected Results for Optical Absorption, Scattering and Extinction Based Instruments.

As listed in Table 1b, the present inter-comparison study included instruments that measure optical absorption, scattering, and extinction. The following real-time absorption instruments were tested: NOAA Photoacoustic Spectrometer (PAS), Photo-Acoustic Soot Spectrometer (PASS-3), and Photo-Thermal Interferometer (PTI). The NOAA PAS and PTI instruments measure absorption at λ = 532 nm. The PASS-3 measures absorption and scattering at λ = 405 nm, 532 nm, and 781 nm.

The real-time extinction instruments tested were the NOAA Cavity Ring Down Aerosol Extinction Spectrometer (CRD-AES) and Cavity Attenuated Phase Shift Extinction Monitor

(CAPS). The CRD-AES instrument operates at three wavelengths, λ = 355 nm, λ = 532 nm, and λ = 1064 nm. The CAPS instrument operates at λ = 445 nm.

The goals for the optically-based instrumentation were to: **(a)** combine the optical and mass-based measurements to obtain the mass specific absorption coefficient (*MAC*) for denuded soot particles; **(b)** determine the effect, if any, of particle shape on absorption and extinction measurements; **(c)** determine the λ-dependence of the σ_{abs} and σ_{ext}; **(d)** determine the effect of non-absorbing coatings (condensed organics from the flame, DOS or H_2SO_4) on σ_{abs}; and **(e)** track changes in the single scattering albedo (SSA) of coated soot particles.

5.1 Performance Study of the PAS, PASS-3 and PTI Instruments.

5.1a Mass Specific Absorption Coefficient for Denuded Soot Particles. The mass specific absorption coefficient (*MAC)* is related to the absorption cross-section and particle mass as shown in Equation 4:

$$\sigma_{abs} = MAC \cdot m_p \qquad (4)$$

The absorption cross-section is typically expressed in units of m^2/particle and the mass specific absorption coefficient in units of m^2/g. Therefore, simultaneous measurements of aerosol absorption, particle number concentration and particle mass provide the parameters necessary for *MAC* determination.

Figure 12 displays σ_{abs} at λ = 532 nm for denuded soot measured with the PASS-3, PTI, and PAS as a function of the mass determined with the CPMA instrument. (Note that σ_{abs} is calculated from ensemble absorption normalized to the particle number concentration.) Three types of denuded particles are shown in the figure: DOS-coated-denuded (green squares),

H_2SO_4-coated-denuded (red circles), and nascent-denuded (black stars). All data shown in Figure 12 are for soot cores generated at $\phi = 2.0 \pm 0.2$ with q1 number fractions ≥ 0.93. Prior to denuding, the DOS and H_2SO_4 coating mass fractions ranged from 0.4-0.99.

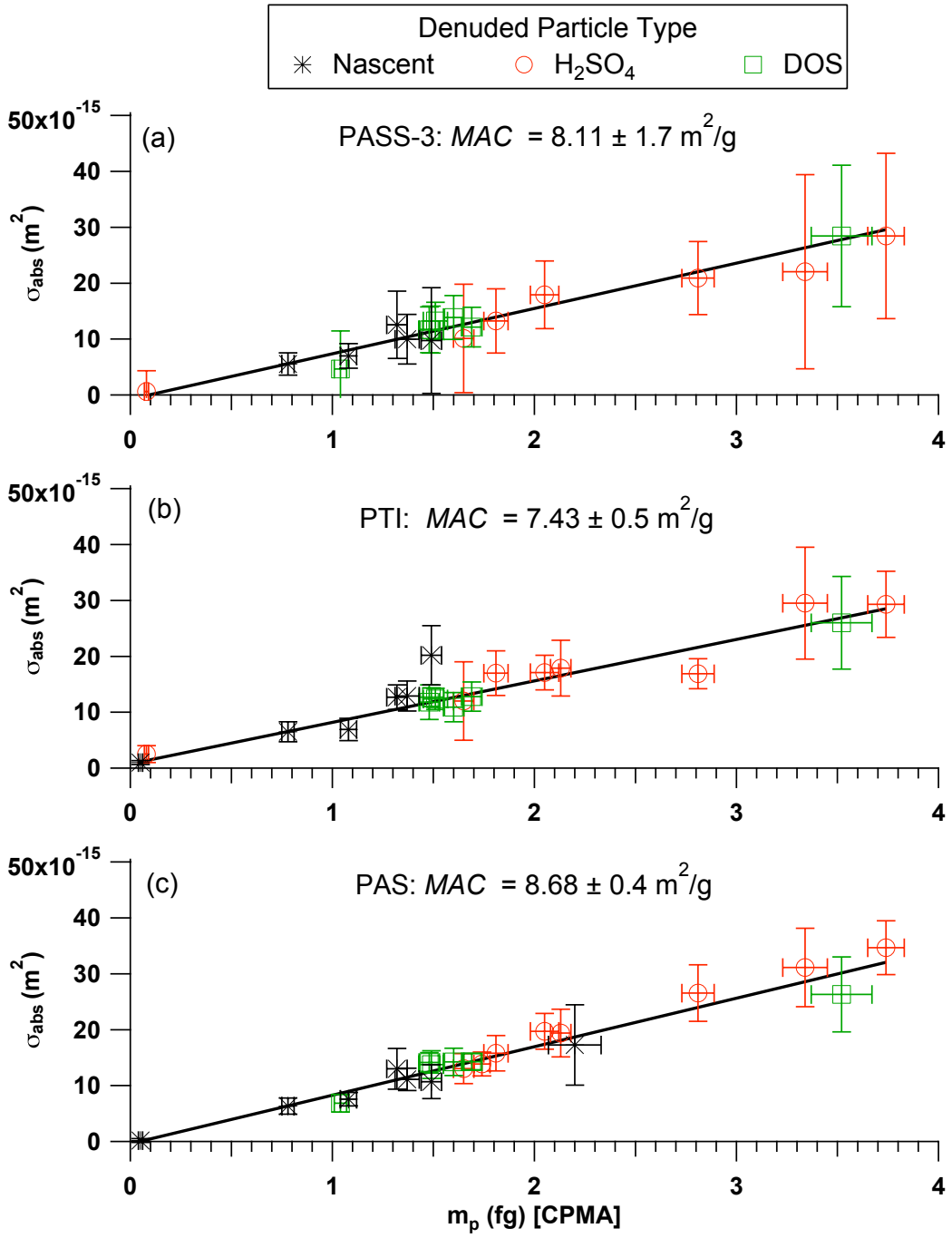

Figures 12. Absorption cross-sections (σ_{abs}) for denuded soot measured at λ = 532 nm for the (a) PASS-3, (b) PTI, and (c) PAS instruments as a function of the mass measured by the CPMA instrument. Soot particles were generated at $\phi = 2.0 \pm 0.2$. The symbols indicate the different coating condition (prior to denuding): DOS-coated-denuded (green squares), H_2SO_4-coated-

denuded (red circles) or nascent-denuded (black stars). The linear regressions shown are fit through all three denuded particle types (weighted to the 1σ standard deviations shown). The slope of each linear fit is the mass specific absorption coefficient (*MAC)*.

The σ_{abs} values together with the CPMA mass measurement yields *MAC* values = 8.11 ± 1.7 m^2/g, 7.43 ± 0.5 m^2/g and 8.68 ± 0.4 m^2/g for the PASS-3, PTI, and PAS respectively. Within experimental accuracy (1σ standard deviation), the *MAC* values obtained with the PASS-3 and PAS instruments are in agreement (8.11 ± 1.7 m^2/g and 8.68 ± 0.4 m^2/g respectively). The *MAC* value provided by the PTI instrument is slightly lower (7.43 ± 0.5 m^2/g) than the *MAC* values obtained with the PASS-3 and PAS instruments. The *MAC* values obtained here for denuded flame-generated soot particles can be compared to *MAC* = 7.5 ± 1.2 m^2/g (at λ = 530 nm) measured for laboratory-generated kerosene soot (*Sheridan et al.* 2005), and a value of *MAC* = 7.5 ± 1.2 m^2/g (at λ = 550 nm) for light absorbing aerosol measured at or near the source. (Compiled from multiple studies in a review by *Bond and Bergstrom* 2006a.) In addition, these results suggest that there is no difference in σ_{abs} resulting from the partial collapse of the fractal soot observed for the H_2SO_4-coated-denuded runs. If this were the case, then the σ_{abs} for the H_2SO_4-coated-dendued trials should fall off the line determined by the nascent-denuded and DOS-coated-denuded trials. Unfortunately, few of the H_2SO_4 points actually overlap with the nascent or DOS points, which would help to strengthen this conclusion. This will be a focus of future studies.

5.2 Wavelength Dependence of σ_{abs} and σ_{ext} for Denuded Soot Particles.

In addition to λ = 532 nm, the PASS-3 also measures absorption at λ = 405 nm and λ = 781 nm. The additional wavelength information is shown in Figure 13 which displays absorption cross-sections for $\lambda = 405$ nm, $\lambda = 532$ nm (repeated from Figure 12), and $\lambda = 781$ nm as a function of the mass measured with the CPMA for denuded soot.

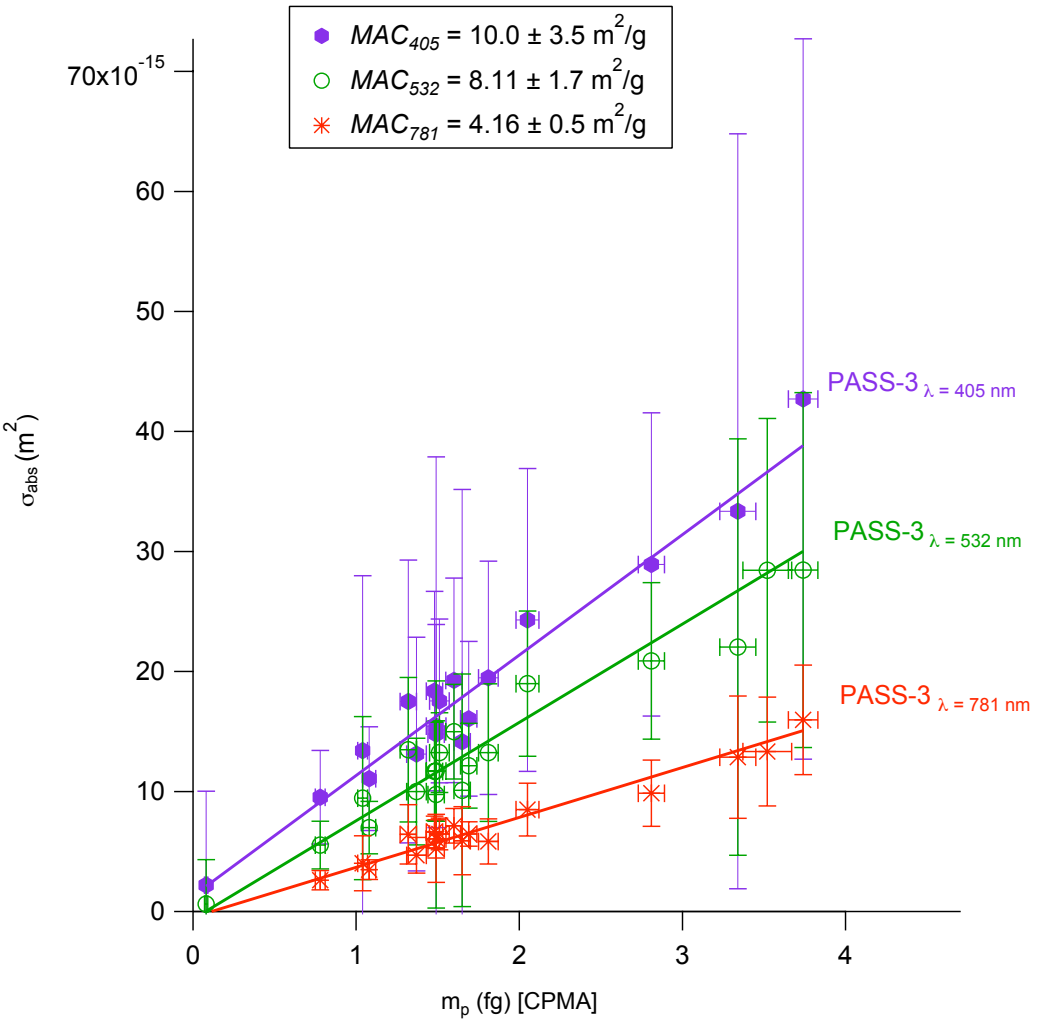

Figure 13. Absorption cross-sections (σ_{abs}) for the PASS-3 at $\lambda = 405$ nm, 532 nm, and 781 nm as a function of CPMA-measured mass for denuded soot particles generated at $\phi = 2.0 \pm 0.2$

(including nascent-denuded, DOS-coated-denuded and H_2SO_4-coated-denuded). The slope of each line is the mass specific absorption coefficient (*MAC*) for the corresponding wavelength.

The *MAC* values are obtained from linear fits to the data (weighted by 1σ standard deviations shown). The PASS-3 data yield *MAC* values of = 10.0 ± 3.5 m^2/g, 8.11 ± 1.7 m^2/g, and 4.16 ± 0.5 m^2/g for the λ = 405 nm, λ = 532 nm, and λ = 781 nm respectively. As shown in the figure, the standard deviations at λ = 405 nm are significantly higher than at λ = 532 nm or λ = 781 nm. The difference in the signal to noise ratios is primarily due to the different laser powers utilized in the PASS-3: ~ 90 mW at λ = 405 nm, ~ 200 mW at λ = 532 nm and ~ 500 mW at 781 nm.

While σ_{abs} is approximately linearly proportional to particle mass (for aerosol particles with a constant refractive index), σ_{ext} (which is the sum of the absorption and scattering cross-sections) will vary more strongly with particle mass (and size). This is due to increased scattering as a function of particle size. Therefore, unlike the *MAC* values obtained in Figure 13, the relationship between σ_{ext} and m_p cannot be characterized with a single mass specific extinction coefficient. However, in the domain where scattering is small (low mass, small size, longer wavelength), the absorption will dominate total extinction and as a result $\sigma_{abs} \sim \sigma_{ext}$.

Two instruments used in the inter-comparison study directly measure extinction: the Cavity Ring Down Aerosol Extinction Spectrometer (CRD-AES) and the Cavity Attenuated Phase Shift Extinction Monitor (CAPS). The CRD-AES instrument measures extinction at λ = 355 nm, λ = 532 nm, and λ = 1064 nm and the CAPS measures extinction at λ = 445 nm. Figure 14 displays σ_{ext} for denuded soot particles as a function of CPMA-measured particle mass. The

CRD-AES data obtained at λ = 355 nm data are excluded from the figure due to a malfunction with the 355 nm photomultiplier.

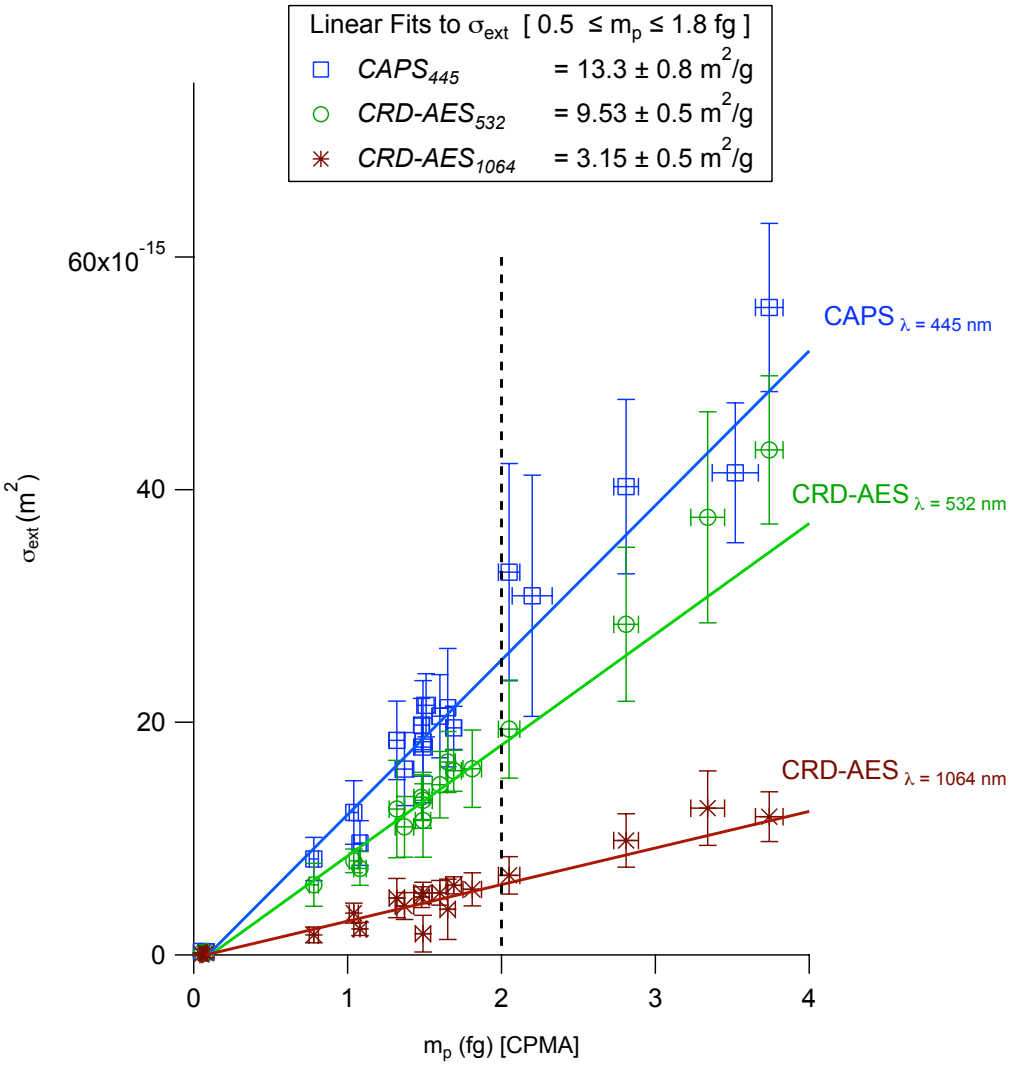

Figure 14. Extinction cross-sections (σ_{ext}) for the CRD-AES instrument at λ = 532 nm, and λ = 1064 nm and for the CAPS instrument at λ = 445 nm as a function of CPMA-measured mass for denuded soot particles generated at ϕ = 2.0 ± 0.2 (including nascent-denuded, DOS-coated-denuded and H_2SO_4-coated-denuded). The error bars shown are the 1σ standard deviation.

The solid lines shown in the figures are the linear fits to the low mass range data from 0.5 $\leq m_p \leq$ 1.8 fg. The vertical dashed line indicates the mass below which data points were fit to the line. The slopes of the linear fits are 13.3 ± 0.8 m^2/g, 9.53 ± 0.5 m^2/g, and 3.15 ± 0.5 m^2/g for λ = 445 nm, λ = 532 nm, and λ = 1064 nm respectively. As expected, the data in Figure 14 show increasing σ_{ext} with increasing particle mass and higher σ_{ext} at lower wavelengths. The deviation of the data points away from the straight lines shown in Figure 14 is attributed to increased scattering. As stated earlier, for denuded soot particles in the low mass range, $\sigma_{abs} \sim \sigma_{ext}$. For the σ_{ext} data obtained with the CRD-AES system at λ = 532 nm the slope of the line shown in Figure 14 (9.53 ± 0.5 m^2/g) can be compared with the *MAC* value of 8.68 ± 0.4 m^2/g obtained with the λ = 532 nm PAS measurements for denuded soot. (The CRD-AES and PAS measurements were made in series during the inter-comparison study.) The slightly higher value obtained with the extinction data suggests that, even within the low mass range, denuded soot particles scatter a small amount of light in addition to their absorption.

5.3 Changes in Absorption and Scattering due to Non-absorbing Coatings on Soot Particles.

Non-absorbing coatings have been reported to enhance the absorption cross-section of BC-containing aerosol particles based on ambient (*Schwarz et al.* 2008; *Shiraiwa et al.* 2008) and laboratory measurements (*Schnaiter et al.* 2005; *Bond et al.* 2006b; *Slowik et al.* 2007a; *Zhang et al.* 2008; *Khalizov et al.* 2009; *Lack et al.* 2009). The enhancement is likely due to lensing effects of the non-absorbing coating that concentrates the light onto the absorbing core. In Figures 15a and 15b we show absorption data for a fractal soot core (d_m = 168 nm) produced

at $\phi = 2.0 \pm 0.2$ as a function of DOS coating thickness. The primary x-axis in each figure is the change in the volume equivalent radius (Δr_{ve}) of the particles. The Δr_{ve} values are calculated from the volume equivalent diameter $d_{ve}/2$ for coated and uncoated soot particles obtained from AMS and SMPS measurements, described in detail in Slowik et al. (2007b). Two additional axes along the top of each graph denote the change in the particle mass (measured with the CPMA) due to DOS coating and the DOS mass fraction. Figure 15a displays the σ_{abs} for the PTI, PAS and PASS-3 instruments. Figure 15b displays the absorption enhancement ($E_{abs} = \sigma_{abs,\ coated} / \sigma_{abs,\ core}$) and shows that E_{abs} increases with increasing DOS coating thickness reaching an enhancement peak of ~ 2 - 2.25 at a DOS coating thickness of Δr_{ve} ~ 100 nm and DOS mass fraction of ~ 0.8 followed by a decrease in absorption for the thickest coating (Δr_{ve} ~ 200 nm). A possible explanation for the observed decrease in absorption enhancement at the thickest coating is the increased scattering by the heavily coated particle partially shielding the absorbing core from the incident light.

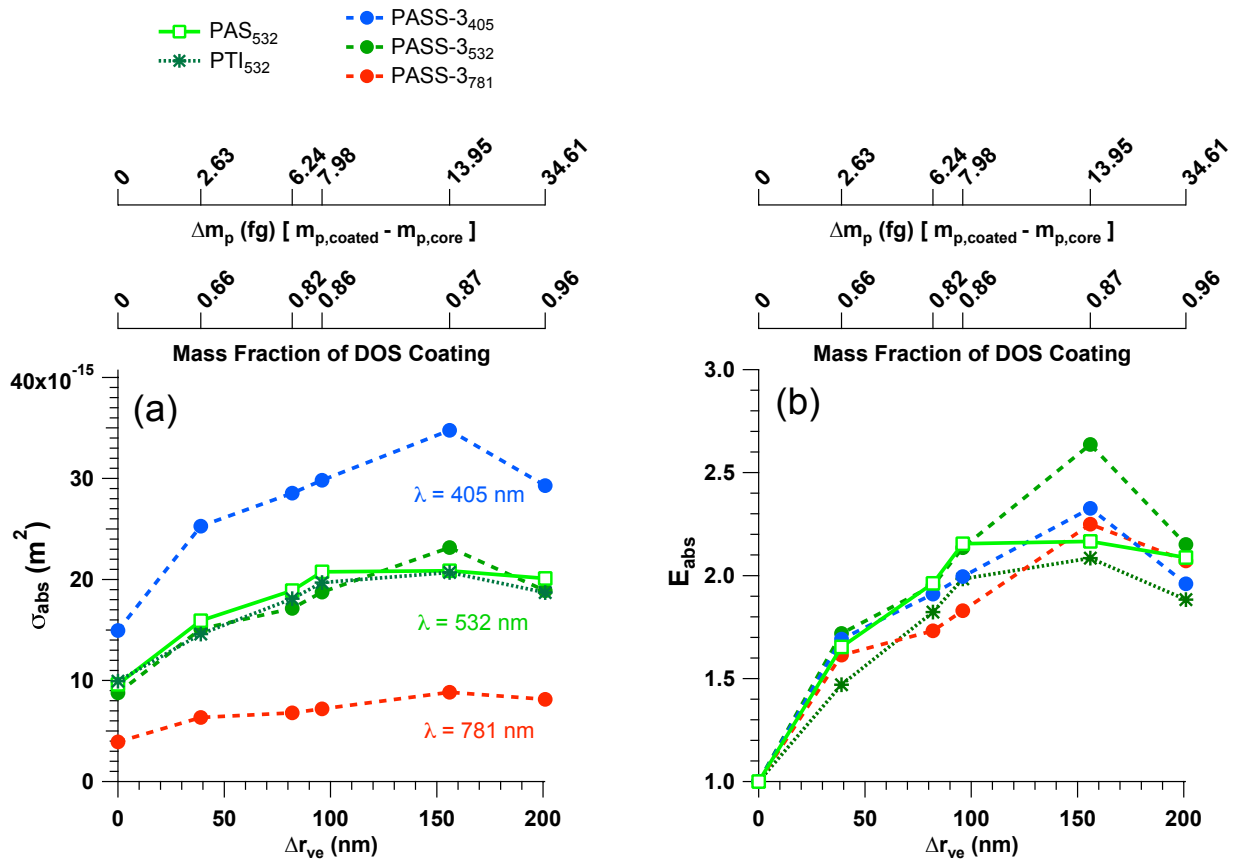

Figure 15. **(a)** Measured absorption cross sections for PASS-781, PASS-532, PASS-405, PTI-532, and PAS-532 instruments for a d_m = 168 nm fractal soot core coated with DOS. **(b)** Ratio of σ_{abs} for the coated particle to σ_{abs} of the core particle corresponding to the data in Figure 16a identifiied by color.

A full range of coating experiments were completed during the inter-comparison including fractal soot cores ranging from d_m = 50 nm to d_m = 209 nm. Each core was systematically coated with DOS or H_2SO_4. In all cases studied, an absorption enhancement of ~ 2 was observed, in line with recent results from Shiraiwa et al. (2010). A detailed presentation of

these results including a comparison with Mie theory core-shell calculations will be provided in a subsequent publication.

To demonstrate the effect of non-absorbing coatings on the SSA of soot particles, Figure 16 shows the change in SSA for the same d_m = 168 nm fractal soot core coated with DOS shown in Figure 15. As in Figure 15, the SSA is plotted here as a function of DOS coating thickness (Δr_{ve}) with additional axes along the top of each graph denoting the change in the particle mass (measured with the CPMA) and mass fraction of the DOS coating.

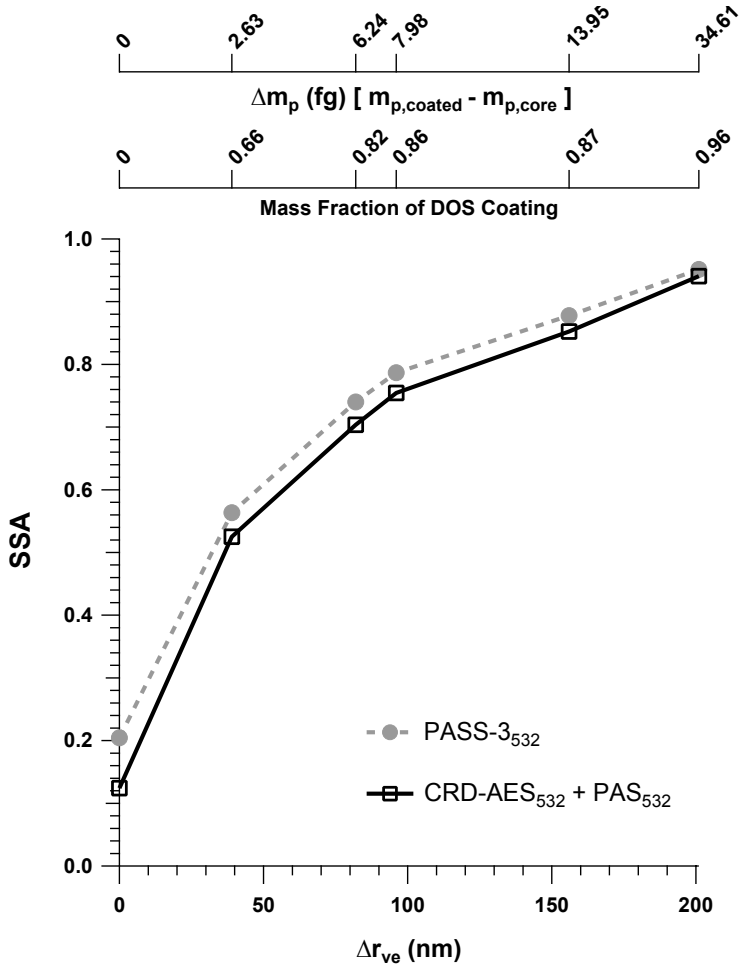

Figure 16. Single scattering albedo (SSA) calculated from the combined CRD-AES/PAS 532 nm data, and the 532 nm PASS-3 data for d_m = 168 nm fractal soot core coated with multiple thicknesses of DOS.

Two SSA curves are shown in Figure 16. One is obtained through the combination of the CRD-AES extinction and PAS absorption data at λ =532 nm and the other is obtained with the λ = 532 nm absorption and scattering measurements of the PASS-3 instrument. The change in SSA obtained with the PASS-3 instrument is in good agreement with the SSA measured with the CRD-AES – PAS instrument combination. The SSA is shown to increase from an initial value of ~ 0.12-0.20 for the nascent d_m = 168 nm soot core to ~ 0.94 for heaviest DOS-coating (DOS mass fraction of 0.96, Δr_{ve} = 201 nm). In comparison to the laboratory SSA values shown here, ambient SSA, determined from scattering and extinction measurements, were reported to vary between 0.60 and 0.85 from early morning to mid-day (*Paredes-Miranda et al.* 2009).

6. Summary.

An inter-comparison study of instruments designed to measure black carbon particle properties was completed. Eighteen instruments were tested, including 7 mass-based (CPMA, AMS-SMPS, SP-AMS, SP2 (3 in number), PAS2000CE) and 9 optically-based (PAS, PTI, PASS-3, CRD-AES, CAPS, MAAP, PSAP (2 in number), Nephelometer) as well as 2 filter samples for OCEC and SEM analyses. The study covered an experimental matrix of 318 runs that systematically tested the performance of each instrument across a range of parameters including: fuel equivalence ratio ($1.8 \leq \phi \leq 5$) particle mobility size ($30 \leq d_m \leq 300$ nm), mass-mobility exponent ($2.0 \leq D_{fm} \leq 3.0$), black carbon mass ($0.07 \leq m_{BC} \leq 4.2$ fg) and particle

chemistry and density (changed via coatings). In coated runs, particles were coated with sulfuric acid or dioctyl sebacate (DOS) ($0.5 \leq \Delta r_{ve} \leq 201$ nm).

Mass measurements provided by the CPMA were validated with PSL particles of known size and density. Coupled CPMA mass measurements for nascent and then denuded soot particles generated at $\phi = 2.0$ and $\phi = 5.0$ provided the black carbon mass in soot produced at different equivalence ratios. Combined CPMA-DMA measurements of m_p and d_m were used to determine the mass-mobility exponent of nascent soot, coated soot, and denuded soot particles. Results indicate that DOS-coated-denuded fractal soot particles substantially retain their fractal aggregate morphology ($D_{fm} = 2.17$) while H_2SO_4-coated-denuded fractal soot particles undergo rearrangement of the fractal core to a more compact morphology ($D_{fm} = 2.49$). Total particle mass measurements with the AMS-SMPS technique compared well with CPMA measurements across the range of particle compositions studied.

Incandescence signals from the three SP2 instruments were calibrated with respect to the CPMA-measured mass for denuded soot particles. Incandescence was found to be independent of particle shape and the type and thickness of non-absorbing coatings studied.

Absorption measurements at $\lambda = 532$ with the PASS-3, PTI, and PAS instruments combined with the CPMA mass measurement provided mass specific absorption coefficients (*MAC*) for denuded soot particles of 8.11 ± 1.7 m^2/g, 7.43 ± 0.5 m^2/g, 8.68 ± 0.4 m^2/g, respectively. Additional *MAC* values of = 10.0 ± 3.5 m^2/g and 4.16 ± 0.5 m^2/g were obtained for denuded soot measured at the $\lambda = 405$ nm and $\lambda = 781$ nm with the PASS-3 instrument.

Extinction measurements with the CAPS ($\lambda = 445$ nm) and CRD-AES ($\lambda = 532$ nm and $\lambda = 1064$ nm) combined with the CPMA mass measurement were used to examine the change in extinction cross-section as a function of mass for denuded soot particles.

Absorption enhancement was observed for a fractal soot core (d_m = 168 nm) coated with DOS. The enhancement reached a plateau of ~ 2 for DOS coating thickness of Δr_{ve} ~ 100 nm and DOS mass fraction > 0.8. The CRD-AES/PAS and PASS-3 instruments were used to measure the single scattering albedo of the DOS-coated d_m = 168 nm fractal soot core. As the thickness of the DOS coating increased the SSA continuously increased, from ~ 0.12 for the nascent soot particles to ~ 0.94 for the thickest DOS coating (Δr_{ve} ~ 201 nm).

ACKNOWLEDGMENTS

This research was supported by the Office of Science (BER), Department of Energy (Atmospheric Science Program) grant No. DE-FG02-05ER63995 and the Atmospheric Chemistry Program of the National Science Foundation grants No. ATM-0525355 and ATM-0854916 to Boston College and Aerodyne Research, Inc. NOAA SP2 participation was supported by the NOAA Atmospheric Composition and Climate, and Health of the Atmosphere Programs, and the NASA Radiation Sciences Program and Upper Atmosphere Research Program. J. Olfert would like to thank Cambustion Ltd. for lending the Couette CPMA for this study. J. Olfert acknowledges the Goldhaber Distinguished Fellowship Program for providing funding for this project. C. Mazzoleni would like to thank MTU for start-up funds for SEM analysis and the Owen P. Mills and Claire F. Drom at the Applied Chemical and Morphological Analysis Laboratory for their support.

REFERENCES

Abu-Rahmah, A., Arnott, W. P. and Moosmuller, H. (2006). Integrating nephelometer with a low truncation angle and an extended calibration scheme. *Measurement Science & Technology* 17:1723-1732.

Allan, J. D., Jimenez, J. L., Williams, P. I., Alfarra, M. R., Bower, K. N., Jayne, J. T., Coe, H. and Worsnop, D. R. (2003). Quantitative sampling using an Aerodyne aerosol mass spectrometer - 1. Techniques of data interpretation and error analysis. . *Journal of Geophysical Research-Atmospheres* 108: NO. D3, 4090, doi:10.1029/2002JD002358

Atkinson, D. B. (2003). Solving chemical problems of environmental importance using cavity ring-down spectroscopy. *Analyst* 128:117-125.

Baynard, T., Lovejoy, E. R., Pettersson, A., Brown, S. S., Lack, D., Osthoff, H., Massoli, P., Bond, T. C., Anderson, T. L. and Campbell, D. (1999). Calibration and intercomparison of filter-based measurements of visible light absorption by aerosols. *Aerosol Science and Technology* 30:582-600.

Bond, T. C. and Bergstrom, R. W. (2006a). Light absorption by carbonaceous particles: An investigative review. *Aerosol Science and Technology* 40:27-67.

Bond, T. C., Habib, G. and Bergstrom, R. W. (2006b). Limitations in the enhancement of visible light absorption due to mixing state. *Journal of Geophysical Research-Atmospheres* 111.

Bulatov, V., Fisher, M. and Schechter, I. (2002). Aerosol analysis by cavity-ring-down laser spectroscopy. *Analytica Chimica Acta* 466:1-9.

Campillo, A. J. and Lin, H. B. (1981). PHOTOTHERMAL SPECTROSCOPY OF AEROSOLS. *Proceedings of the Society of Photo-Optical Instrumentation Engineers* 286:24-32.

Canagaratna, M. R., Jayne, J. T., Ghertner, D. A., Herndon, S., Shi, Q., Jimenez, J. L., Silva, P. J., Williams, P., Lanni, T., Drewnick, F., Demerjian, K. L., Kolb, C. E. and Worsnop, D. R. (2004). Chase studies of particulate emissions from in-use New York City vehicles. *Aerosol Science and Technology* 38:555-573.

Canagaratna, M. R., Jayne, J. T., Jimenez, J. L., Allan, J. D., Alfarra, M. R., Zhang, Q., Onasch, T. B., Drewnick, F., Coe, H., Middlebrook, A., Delia, A., Williams, L. R., Trimborn, A. M., Northway, M. J., DeCarlo, P. F., Kolb, C. E., Davidovits, P. and Worsnop, D. R. (2007). Chemical and microphysical characterization of ambient aerosols with the aerodyne aerosol mass spectrometer. *Mass Spectrometry Reviews* 26:185-222.

Chakrabarty, R. K., Moosmuller, H., Arnott, W. P., Garro, M. A., Tian, G. X., Slowik, J. G., Cross, E. S., Han, J. H., Davidovits, P., Onasch, T. B. and Worsnop, D. R. (2009). Low Fractal Dimension Cluster-Dilute Soot Aggregates from a Premixed Flame. *Physical Review Letters* 102.

Chakrabarty, R. K., Moosmuller, H., Garro, M. A., Arnott, W. P., Walker, J., Susott, R. A., Babbitt, R. E., Wold, C. E., Lincoln, E. N. and Hao, W. M. (2006). Emissions from the laboratory combustion of wildland fuels: Particle morphology and size. *Journal of Geophysical Research-Atmospheres* 111: D07204, doi:10.1029/2005JD006659

Cross, E. S., Onasch, T. B., Canagaratna, M., Jayne, J. T., Kimmel, J., Yu, X. Y., Alexander, M. L., Worsnop, D. R. and Davidovits, P. (2009). Single particle characterization using a light scattering module coupled to a time-of-flight aerosol mass spectrometer. *Atmospheric Chemistry and Physics* 9:7769-7793.

Cross, E. S., Slowik, J. G., Davidovits, P., Allan, J. D., Worsnop, D. R., Jayne, J. T., Lewis, D. K., Canagaratna, M. and Onasch, T. B. (2007). Laboratory and ambient particle density

determinations using light scattering in conjunction with aerosol mass spectrometry. *Aerosol Science and Technology* 41:343-359.

Curtius, J., Sierau, B., Arnold, F., Baumann, R., Busen, R., Schulte, P. and Schumann, U. (1998). First direct sulfuric acid detection in the exhaust plume of a jet aircraft in flight. *Geophysical Research Letters* 25: NO. D6, 923-926.

Davis, C. C. (1980). Trace Detection in Gases using Phase Fluctuation Optical Heterodyne Spectroscopy. *Applied Physics Letters* 36:515-518.

DeCarlo, P. F., Slowik, J. G., Worsnop, D. R., Davidovits, P. and Jimenez, J. L. (2004). Particle morphology and density characterization by combined mobility and aerodynamic diameter measurements. Part 1: Theory. *Aerosol Science and Technology* 38:1185-1205.

Fluckiger, D. U., Lin, H. B. and Marlow, W. H. (1985). Composition Measurement of Aerosols of Submicrometer Particles by Phase Fluctuation Absorption-Spectroscopy. *Applied Optics* 24:1668-1681.

Grieshop, A. P., Reynolds, C. C. O., Kandlikar, M. and Dowlatabadi, H. (2009). A black-carbon mitigation wedge. *Nature Geoscience* 2:533-534.

Hansen, A. D. A., Rosen, H. and Novakov, T. (1984). The Aethalometer - an Instrument for the Real-Time Measurement of Optical-Absorption by Aerosol Particles. *Science of the Total Environment* 36:191-196.

Heintzenberg, J. and Charlson, R. J. (1996). Design and applications of the integrating nephelometer: A review. *Journal of Atmospheric and Oceanic Technology* 13:987-1000.

Huffman, J. A., Ziemann, P. J., Jayne, J. T., Worsnop, D. R. and Jimenez, J. L. (2008). Development and characterization of a fast-stepping/scanning thermodenuder for chemically-resolved aerosol volatility measurements. *Aerosol Science and Technology*

42:395-407.

Jacobson, M. Z. (2001). Strong radiative heating due to the mixing state of black carbon in atmospheric aerosols. *Nature* 409:695-697.

Jayne, J. T., Leard, D. C., Zhang, X. F., Davidovits, P., Smith, K. A., Kolb, C. E. and Worsnop, D. R. (2000). Development of an aerosol mass spectrometer for size and composition analysis of submicron particles. *Aerosol Science and Technology* 33:49-70.

Jiang, M., Marr, L. C., Dunlea, E. J., Herndon, S. C., Jayne, J. T., Kolb, C. E., Knighton, W. B., Rogers, T. M., Zavala, M., Molina, L. T. and Molina, M. J. (2005). Vehicle fleet emissions of black carbon, polycyclic aromatic hydrocarbons, and other pollutants measured by a mobile laboratory in Mexico City. *Atmospheric Chemistry and Physics* 5:3377-3387.

Jimenez, J. L., Jayne, J. T., Shi, Q., Kolb, C. E., Worsnop, D. R., Yourshaw, I., Seinfeld, J. H., Flagan, R. C., Zhang, X. F., Smith, K. A., Morris, J. W. and Davidovits, P. (2003). Ambient aerosol sampling using the Aerodyne Aerosol Mass Spectrometer. *Journal of Geophysical Research-Atmospheres* 108: NO. D7, 8425, doi:10.1029/2001JD001213

Kebabian, P. L., Robinson, W. A. and Freedman, A. (2007). Optical Extinction Monitor Using CW Cavity Enhanced Detection. *Review of Scientific Instruments* 78, 063102, doi:10.1063/1.2744223

Khalizov, A. F., Xue, H. X., Wang, L., Zheng, J. and Zhang, R. Y. (2009). Enhanced Light Absorption and Scattering by Carbon Soot Aerosol Internally Mixed with Sulfuric Acid. *Journal of Physical Chemistry A* 113:1066-1074.

Kittelson, D. B. (1998). Engines and nanoparticles: A review. *Journal of Aerosol Science* 29:575-588.

Koylu, U. O., Faeth, G. M., Farias, T. L., and Carvalho, M. G. (1995). Fractal and projected structure properties of soot aggregates, *Combusion and Flame*, 100:621-633.

Kutz, S., and Schmidt-Ott, A. (1992). Characterization of Agglomerates by Condensation-

Induced Restructuring, *Journal of Aerosol Science*. 23:S357–S360.

Kuwata, M., Kondo, Y. and Takegawa, N. (2009). Critical condensed mass for activation of black carbon as cloud condensation nuclei in Tokyo. *Journal of Geophysical Research-Atmospheres* 114: D20202, doi:10.1029/2009JD012086

Lack, D. A., Cappa, C. D., Cross, E. S., Massoli, P., Ahern, A. T., Davidovits, P. and Onasch, T. B. (2009). Absorption Enhancement of Coated Absorbing Aerosols: Validation of the Photo-Acoustic Technique for Measuring the Enhancement. *Aerosol Science and Technology* 43:1006-1012.

Marr, L. C., Grogan, L. A., Wohrnschimmel, H., Molina, L. T., Molina, M. J., Smith, T. J. and Garshick, E. (2004). Vehicle traffic as a source of particulate polycyclic aromatic hydrocarbon exposure in the Mexico City metropolitan area. *Environmental Science & Technology* 38:2584-2592.

Massoli, P., Kebabian, P.L., Onasch, T.B., Hills, F.B. and Freedman, A. (2010) Aerosol light extinction measurements by Cavity Attenuated Phase Shift Spectroscopy (CAPS): laboratory validation and field deployment of a compact aerosol extinction monitor, *Aerosol Science and Technology, in press.*

Moosmuller, H., Chakrabarty, R. K. and Arnott, W. P. (2008). Aerosol light absorption and its measurement: A review, in *Annual Meeting of the Association-for-Aerosol-Research*, Karlsruhe, GERMANY, 844-878.

Moosmuller, H., Varma, R. and Arnott, W. P. (2005). Cavity ring-down and cavity-enhanced detection techniques for the measurement of aerosol extinction. *Aerosol Science and Technology* 39:30-39.

Murphy, D. M., Cziczo, D. J., Froyd, K. D., Hudson, P. K., Matthew, B. M., Middlebrook, A.

M., Peltier, R. E., Sullivan, A., Thomson, D. S. and Weber, R. J. (2006). Single-particle mass spectrometry of tropospheric aerosol particles. *Journal of Geophysical Research-Atmospheres* 111: D23S32, doi:10.1029/2006JD007340

Olfert, J. S. and Collings, N. (2005). New method for particle mass classification - the Couette centrifugal particle mass analyzer. *Journal of Aerosol Science* 36:1338-1352.

Onasch, T. B., Jayne, J. T., Herndon, S., Worsnop, D. R., Miake-Lye, R. C., Mortimer, I. P. and Anderson, B. E. (2009). Chemical Properties of Aircraft Engine Particulate Exhaust Emissions. *Journal of Propulsion and Power* 25:1121-1137.

Pagels, J., Khalizov, A. F., McMurry, P. H. and Zhang, R. Y. (2009). Processing of Soot by Controlled Sulphuric Acid and Water Condensation-Mass and Mobility Relationship. *Aerosol Science & Technology*. 43:629 - 640.

Paredes-Miranda, G., Arnott, W. P., Jimenez, J. L., Aiken, A. C., Gaffney, J. S. and Marley, N. A. (2009). Primary and secondary contributions to aerosol light scattering and absorption in Mexico City during the MILAGRO 2006 campaign. *Atmospheric Chemistry and Physics* 9:3721-3730.

Park, K., Cao, F., Kittelson, D. B. and McMurry, P. H. (2003). Relationship between particle mass and mobility for diesel exhaust particles. *Environmental Science & Technology* 37:577-583.

Park, K., Kittelson, D. B., and McMurry, P. H. (2004). Structural properties of diesel exhaust particles measured by transmission electron microscopy (TEM): Relationships to particle mass and mobility, Aerosol Sci. Technol., 38:881-889.

Park, K., Dutcher, D., Emery, M., Pagels, J., Sakurai, H., Scheckman, J., Qian, S., Stolzenburg, M. R., Wang, X., Yang, J. and McMurry, P. H. (2008). Tandem measurements of aerosol

properties - A review of mobility techniques with extensions. *Aerosol Science and Technology* 42:801-816.

Pettersson, A., Lovejoy, E. R., Brock, C. A., Brown, S. S. and Ravishankara, A. R. (2004). Measurement of aerosol optical extinction at 532nm with pulsed cavity ring down spectroscopy. *Journal of Aerosol Science* 35:995-1011.

Petzold, A., Schloesser, H., Sheridan, P. J., Arnott, W. P., Ogren, J. A. and Virkkula, A. (2005). Evaluation of multiangle absorption photometry for measuring aerosol light absorption. *Aerosol Science and Technology* 39:40-51.

Petzold, A. and Schonlinner, M. (2004). Multi-angle absorption photometry - a new method for the measurement of aerosol light absorption and atmospheric black carbon. *Journal of Aerosol Science* 35:421-441.

Ramanathan, V. and Carmichael, G. (2008). Global and regional climate changes due to black carbon. *Nature Geoscience* 1:221-227.

Ramanathan, V., Crutzen, P. J., Kiehl, J. T. and Rosenfeld, D. (2001). Atmosphere - Aerosols, climate, and the hydrological cycle. *Science* 294:2119-2124.

Ramanathan, V. and Feng, Y. (2009). Air pollution, greenhouse gases and climate change: Global and regional perspectives. *Atmospheric Environment* 43:37-50.

Rypdal, K., Rive, N., Berntsen, T. K., Klimont, Z., Mideksa, T. K., Myhre, G. and Skeie, R. B. (2009). Costs and global impacts of black carbon abatement strategies. *Tellus Series B-Chemical and Physical Meteorology* 61:625-641.

Sakurai, H., Tobias, H. J., Park, K., Zarling, D., Docherty, S., Kittelson, D. B., McMurry, P. H. and Ziemann, P. J. (2003). On-line measurements of diesel nanoparticle composition and volatility. *Atmospheric Environment* 37:1199-1210.

Schmidt-Ott, A., Baltensperger, U., Gaggeler, H. W., and Jost, D. T. (1990). Scaling behavior of physical parameters describing agglomerates, *Journal of Aerosol Science*., 21(6):711-717.

Schnaiter, M., Linke, C., Mohler, O., Naumann, K. H., Saathoff, H., Wagner, R., Schurath, U. and Wehner, B. (2005). Absorption amplification of black carbon internally mixed with secondary organic aerosol. *Journal of Geophysical Research-Atmospheres* 110: D19204, doi:10.1029/2005JD006046

Schwartz, S. E. and Buseck, P. R. (2000). Atmospheric science - Absorbing phenomena. *Science* 288:989-990.

Schwarz, J. P., Gao, R. S., Fahey, D. W., Thomson, D. S., Watts, L. A., Wilson, J. C., Reeves, J. M., Baumgardner, D. G., Kok, G. L., Chung, S., Schulz, M., Hendricks, J., Lauer, A., K¨archer, B., Slowik, J. G., Rosenlof, K. H., Thompson, T. L., Langford, A. O., Lowenstein, M., and Aikin, K. C. (2006). Single-Particle Measurements of Midlatitude Black Carbon and Light-Scattering Aerosols from the Boundary Layer to the Lower Stratosphere. *J. Geophys. Res.* 111:D16207. doi:10.1029/2006JD007076.

Schwarz, J. P., Spackman, J. R., Fahey, D. W., Gao, R. S., Lohmann, U., Stier, P., Watts, L. A., Thomson, D. S., Lack, D. A., Pfister, L., Mahoney, M. J., Baumgardner, D., Wilson, J. C. and Reeves, J. M. (2008). Coatings and their enhancement of black carbon light absorption in the tropical atmosphere. *Journal of Geophysical Research-Atmospheres* 113:D03203, doi:10.1029/2007JD009042.

Schwarz, J. P., Spackman, J. R., Gao, R. S., Perring, A. E., Cross, E.S., Onasch, T. B., Ahern, A., Wrobel, W., Davidovits, D., Olfert, J., Dubey, M. K., Mazzoleni, C. and Fahey, D. W. (2010). The detection efficiency of the single particle soot photometer. Submitted to *Aerosol Science and Technology*.

Sedlacek, A. J. (2006). Real-time detection of ambient aerosols using photothermal interferometry: Folded Jamin interferometer. *Review of Scientific Instruments* 77.

Sedlacek, A. and Lee, J. (2007). Photothermal interferometric aerosol absorption spectrometry. *Aerosol Science and Technology* 41:1089-1101.

Seinfeld, J. H., S. N. Pandis (2006). *Atmospheric Chemistry and Physics: From Air Pollution to Climate Change*. John Wiley & Sons, Inc., New York.

Shiraiwa, M., Kondo, Y., Iwamoto, T. and Kita, K. (2010). Amplification of Light Absorption of Black Carbon by Organic Coating. *Aerosol Science and Technology* 44:46 - 54.

Shiraiwa, M., Kondo, Y., Moteki, N., Takegawa, N., Sahu, L. K., Takami, A., Hatakeyama, S., Yonemura, S. and Blake, D. R. (2008). Radiative impact of mixing state of black carbon aerosol in Asian outflow. *Journal of Geophysical Research-Atmospheres* 113: D24210, doi:10.1029/2008JD010546

Slowik, J. G., Cross, E. S., Han, J. H., Davidovits, P., Onasch, T. B., Jayne, J. T., WilliamS, L. R., Canagaratna, M. R., Worsnop, D. R., Chakrabarty, R. K., Moosmuller, H., Arnott, W. P., Schwarz, J. P., Gao, R. S., Fahey, D. W., Kok, G. L. and Petzold, A. (2007a). An inter-comparison of instruments measuring black carbon content of soot particles. *Aerosol Science and Technology* 41:295-314.

Slowik, J. G., Cross, E. S., Han, J. H., Kolucki, J., Davidovits, P., Williams, L. R., Onasch, T. B., Jayne, J. T., Kolb, C. E. and Worsnop, D. R. (2007b). Measurements of morphology changes of fractal soot particles using coating and denuding experiments: Implications for optical absorption and atmospheric lifetime. *Aerosol Science and Technology* 41:734-750.

Slowik, J. G., Stainken, K., Davidovits, P., Williams, L. R., Jayne, J. T., Kolb, C. E., Worsnop, D. R., Rudich, Y., DeCarlo, P. F. and Jimenez, J. L. (2004). Particle morphology and density

characterization by combined mobility and aerodynamic diameter measurements. Part 2: Application to combustion-generated soot aerosols as a function of fuel equivalence ratio. *Aerosol Science and Technology* 38:1206-1222.

Smith, J. D. and Atkinson, D. B. (2001). A portable pulsed cavity ring-down transmissometer for measurement of the optical extinction of the atmospheric aerosol. *Analyst* 126:1216-1220.

Stephens, M., Turner, N. and Sandberg, J. (2003). Particle identification by laser-induced incandescence in a solid-state laser cavity. *Applied Optics* 42:3726-3736.

Strawa, A. W., Castaneda, R., Owano, T., Baer, D. S. and Paldus, B. A. (2003). The measurement of aerosol optical properties using continuous wave cavity ring-down techniques. *Journal of Atmospheric and Oceanic Technology* 20:454-465.

Wang, G. M., and Sorensen, C. M. (1999). Diffusive mobility of fractal aggregates over the entire knudsen number range, Phys. Rev. E 60(3):3036-3044.

Zhang, R. Y., Khalizov, A. F., Pagels, J., Zhang, D., Xue, H. X. and McMurry, P. H. (2008). Variability in morphology, hygroscopicity, and optical properties of soot aerosols during atmospheric processing. *Proceedings of the National Academy of Sciences of the United States of America* 105:10291-10296.

APPENDIX

Description of Instruments. Several of the instruments in the study are relatively well developed and have been in use for several years. For these instruments, the objectives of the inter-comparison work were to verify instrument assumptions and to confirm the published limits of operation for each instrument. Other instruments in the study were newly designed and not yet fully tested. For the new instruments, this study aimed at validating concepts, highlighting capabilities and providing information required for further instrument development.

In this appendix, we provide a brief description of the instruments listed in Tables 1a and b. Details of instrument design and operation are found in the cited references.

A. Mass Based Instruments.

Aerosol Mass Spectrometer-Scanning Mobility Particle Sizer (AMS-SMPS). (*Slowik et al.* 2004; *DeCarlo et al.* 2004) This apparatus is a combination of two stand-alone instruments; the Aerodyne Aerosol Mass Spectrometer (AMS) and the Scanning Mobility Particle Sizer (SMPS) manufactured by TSI. The Aerodyne AMS consists of three main sections: (1) aerodynamic lens inlet, (2) time of flight region and (3) particle vaporizer and mass spectrometer (*Jayne et al.* 2000; *Allan et al.* 2003; *Jimenez et al.* 2003). Particles enter the AMS through a 100 μm orifice and pass through a series of aerodynamic lenses that focus the particles into a narrow beam. The pressure drop at the lens exit accelerates the particles to a velocity inversely related to their vacuum aerodynamic diameter (d_{va}). The velocity calibration of the AMS is obtained with PSL particles of known size, shape, and density as described in Jayne et al. (2000). The particles strike a heated surface where the non-refractory components are flash vaporized at a temperature

T ~ 600°C. The resulting vapor is ionized by electron impact (70 eV) and detected by a time-of-flight mass spectrometer.

The AMS used in this study was also equipped with an optical detection module, which functions as an additional particle detector providing a more accurate determination of particle d_{va} for both refractory and non-refractory particles (*Cross et al.* 2007; *Cross et al.* 2009).

The SMPS part of the instrument is a combination of a differential mobility analyzer (DMA) (Model 3080, TSI Inc., St. Paul, MN, USA) and a condensation particle counter (CPC) (Model 3010, TSI Inc.). The DMA scans through the particle size distribution with a period of two minutes, while the CPC counts the number of particles in each size bin. The SMPS measures the particle mobility diameter (d_m) and total particle concentration in the flow. The empirical relationship between DMA-column voltage and particle mobility was calibrated with PSL particles of known diameter. By comparing the mobility diameter before and after particle processing, coating thickness (Δd_m) can be determined.

The AMS alone does not detect the refractory content of aerosol particles. However, the combined measurements of the AMS and SMPS provide complementary information about the aerosol particles that allows one to deduce the refractory mass. Using equations presented in DeCarlo et al. 2004 and Slowik et al. 2004, the coupled AMS-SMPS measurements of d_m, d_{va}, and the non-refractory composition of the particles can be combined with estimates of particle material density to yield particle mass, dynamic shape factor (χ), and chemical composition (including the refractory component).

The Couette Centrifugal Particle Mass Analyzer. (CPMA). (*Olfert and Collings,* 2005) The Couette Centrifugal Particle Mass Analyzer (CPMA) consists of two coaxial cylindrical electrodes rotating at different angular velocities. Pre-charged particles pass between the

electrodes where electrostatic and centrifugal forces act in opposite directions. Particles also experience a drag force that opposes the direction of motion. Particles of a specific mass-to-charge ratio pass through the CPMA, depending on the rotational speed and voltage difference between the electrodes. If the charge on the particles is known, the mass of the transmitted particles is determined independent of particle shape. During this study, the CPMA was operated in front of one of two CPC's configured to sample in parallel. This setup enabled accurate mass-per-particle measurements for mobility-selected particles without concern for variations in the number concentration of the sampled particles.

The CPMA mass data combined with the known mobility diameter of the particles yields a measure of the mass-mobility exponent (D_{fm}) of the particles.

Single Particle Soot Photometer (SP2). (*Stephens et al.* 2003; *Schwarz et al.* 2006) In the SP2 instrument, single particles intersect an intense, intra-cavity, continuous Nd:YAG laser beam (λ = 1064 nm). The infrared radiation is absorbed by black carbon (i.e. absorbing component of a sampled soot particle) and heats the particle to approximately 4000 K, vaporizating nonrefractory materials (if any) in the process.. The remaining, hot black carbon core emits substantial thermal radiation in the visible (i.e. incandesces). The incandescence signal is measured over two wavelength bands as the particle transits the laser beam and the maximum light intensity in each channel is recorded (i.e. peak height). The ratio of the two wavelength bands is used to determine the particle vaporization temperature (or "color") and the magnitude of the incandescence signals are correlated with the black carbon mass in the particle. The three SP2 instruments used in these experiments were operated respectively by NOAA CSD, Droplet Measurement Technologies (DMT) and the University of Hawaii.

Soot Particle-Aerosol Mass Spectrometer (SP-AMS). (In development by Aerodyne Research and Droplet Measurement Technologies.) The SP-AMS is a combination of the SP2 and the AMS instruments. The SP2 instrument is designed to provide a quantitative measure of the refractory mass but yields little information about the chemical composition of the particle. The AMS on the other hand, measures the particle chemical composition but, as a stand-alone instrument it does not detect refractory mass. In this instrument combination, the thermal vaporizer of the AMS is replaced with an intra-cavity 1064 nm laser beam. The SP-AMS instrument utilizes the laser-induced incandescence of absorbing soot particles to vaporize both the coatings and elemental carbon cores within the ionization region of the AMS, providing a method for measuring the mass spectral signals from both refractory and non-refractory components of the aerosol particles. The instrument also provides a measure of the aerosol d_{va}.

Photoelectric Aerosol Sensor of Particle-bound PAH (PAS2000CE). *(EcoChem Analytics)* In this instrument, UV light from an excimer lamp source is used to photoionize highly conjugated aromatic molecules (e.g. polycyclic aromatic hydrocarbons or PAH's) on the surface of soot particles. The electrons produced are removed with an electric field and the positively charged particles are collected on a filter inside an electrometer where the charge is monitored. The measured electric current is proportional to the concentration of particle-bound PAH's.

B. Optically Based Instruments

Photoacoustic Spectrometer (PAS). (*Lack et al.* 2006) In the PAS instrument, particles are irradiated by laser light (λ = 532 nm) modulated as a square wave at ~1 kHz. The absorbed laser light heats the particles and the heat produced within the particles is rapidly transferred to the surrounding gas. The resulting pressure increase forms a standing acoustic wave that is detected

by a microphone. The PAS simultaneously monitors a particle-free channel to reduce and remove interfering noise effects. The acoustic response of the PAS is calibrated using the CRD-AES as a reference. Specifically, an absorbing gas (here, O_3) is passed through the CRD-AES to the PAS. The CRD-AES provides an absolute measure of the absorption by the gas and the PAS is referenced to this simultaneously measured value. Calibrations of the PAS were performed 1-2 times per day using absorption levels which were of the same order as the values observed during the soot experiments.

Photoacoustic Soot Spectrometer (PASS-3). (*Arnott et al.* 1999, *Flowers et al.* Submitted to GRL, 2009) The PASS-3 is a new instrument manufactured by DMT; it operates on the same principle as the PAS to measure aerosol absorption. The PASS-3 used in the current study measures β_{abs} at λ = 405 nm, 532 nm and 781 nm. The three lasers are modulated at different frequencies (centered around ~1.5 KHz) within the frequency response of an acoustic resonator. In addition to measuring absorption at each wavelength, the PASS-3 instrument also measures the integrated scattered light (β_{sca}) with a truncation angle of ~5^o in both the forward and backward directions; the scattering measurement is synchronously performed on the same sampling volume as the one used for the absorption measurement. Scattered light is measured by employing a reciprocal nephelometer approach and by using a Lambertian diffuser mounted in the middle-point of the acoustic resonator. Gases interferences and other background signals are removed by automated and frequent collection of filtered (HEPA) air.

The PASS-3 is calibrated by first introducing non-absorbing ammonium sulfate particles at very high mass loadings (β_{ext} ~1,000 ~30,0000 Mm^{-1}). An integrating sphere inside PASS-3 measures extinction by the ammonium sulfate particles and the scattering module is calibrated to this value. Ammonium sulfate is non-absorbing and generates no photoacoustic signal, therefore

$\beta_{ext} \sim \beta_{sca}$ (small particles are used so truncation errors can be neglected). High mass loadings are necessary because the extinction measurement is made using Beer's Law from a single pass through the photoacoustic cell. Following this, absorbing aerosol (e.g. soot generated in a kerosene lamp, or spherocarbs) is introduced and the absorption calibration coefficient is determined from the difference between the measured extinction and the calibrated scattering, again at high mass loadings. Due to the high linearity of the detectors, the calibration is extrapolated to the entire measurement range (including low signals). The PASS-3 was calibrated using this procedure at DMT prior to the inter-comparison study and again in the laboratory at the Los Alamos National Laboratory after the study, without any significant change. Although this closure calibration procedure is appropriate and standard for single-cell photoacoustic instruments, as a confirmation we performed an additional absolute calibration of the absorption system during the inter-comparison experiment. For this we used low concentrations of NO_2 ($\beta_{abs} < 80$ Mm^{-1} at $\lambda = 532$ nm and $\beta_{abs} < 280$ Mm^{-1} at $\lambda = 405$ nm). This absolute calibration does not rely on the extinction measurement and can be performed at low signals to verify the linearity of the system as well as provide an independent calibration method. NO_2 absorbs at $\lambda = 405$ nm and $\lambda = 532$ nm allowing simultaneous calibration of the absorption channel at these two wavelengths. The absolute calibration at low NO_2 concentrations resulted in the following calibration slopes relative to the standard closure calibration: 0.97 ± 0.22 for the $\lambda = 532$ nm channel and 1.02 ± 0.18 for the $\lambda = 405$nm channel, where the uncertainties represent a 95% confidence interval reflecting the noise in the data at low signal and the uncertainty in the NO_2 concentrations.

Photo-Thermal interferometer (PTI). (*Sedlacek,* 2006; *Sedlacek and Lee,* 2007). The PTI

technique measures the *optical* pathlength change that one arm of an interferometer (referred to as the 'probe' arm) experiences relative to the other arm of the interferometer (called the 'reference' arm). When the two arms are recombined at a beamsplitter, an interference pattern is created. If the optical pathlength in one arm of the interferometer changes, a commensurate shift in the interference pattern will take place. For the specific application of measuring light absorption, the heating of air surrounding the light- absorbing aerosol following laser illumination induces the optical pathlength change. This localized heating creates a refractive index gradient causing the probe arm of the interferometer to take a slightly different *optical* pathlength relative to the unperturbed reference arm. This effect is analogous to solar heating of a road causing mirages. This altered optical pathlength results in a shift in the interference pattern that is then detected as a change in the signal intensity by a single element detector. The current optical arrangement utilizes a folded Jamin interferometer design. Currently the PTI operates at $\lambda = 532$ nm.

The PTI instrument is calibrated by injecting a known concentration of an absorbing gas (i.e. NO_2) into the sample cell and recording the resultant signal as a function of gas concentration. The absorption cross-section of the calibration gas must be known and the gas not undergo photolysis at the interrogation wavelength of $\lambda = 532$ nm.

A Cavity Ring Down Aerosol Extinction Spectrometer (CRD-AES). (*Baynard et al.* 2007) In the pulsed cavity ring-down instrument, a laser pulse is coupled into an optical cavity formed by a pair of high reflectivity mirrors. Scattering and absorption by particles (also gases) reduces the lifetime of the light within the cavity. The light intensity decays exponentially with a time constant τ proportional to losses within the cavity and at the mirrors. The aerosol extinction (β_{ext}) is obtained from the measured decay time at three wavelengths: $\lambda = 355$ nm, 532 nm, and

1064 nm (in three separate cells). The instrument also has two additional two cavity ring-down cells to determine the RH dependence of the extinction coefficient at 532 nm through independent RH control of the two ring-down cells (RH = 60% and 85%).

Cavity Attenuated Phase Shift Extinction Monitor (CAPS). (*Kebabian et al.* 2007; *Massoli et al.* 2009; - In development at Aerodyne Research) The CAPS-based optical extinction monitor employs a variant of cavity-enhanced detection called cavity attenuated phase shift spectroscopy. The CAPS extinction monitor comprises a light emitting diode (LED), an optical cavity employing a near confocal arrangement of high reflectivity (R>0.9998) mirrors that acts as the sample cell, and a vacuum photodiode for light detection. The light extinction is determined from changes in the phase shift of the distorted waveform of the square-wave modulated LED light that is transmitted through the optical cell. The magnitude of the phase shift is a function of fixed instrument properties (i.e. cell length, mirror reflectivity, and modulation frequency) and light extinction within the cell. Particle-free air is systematically sampled to subtract gas phase interferences and the effect of the fixed instrument properties. The instrument in the present study employed a royal blue LED in conjunction with a bandpass filter resulting in a light beam with a center wavelength of 445 nm and spectral width of ±5 nm.

Nephelometer (*Heintzenberg and Charlson*, 1996 and references therein) The nephelometer used in this study measures the total light scattered (β_{sca}) by the aerosol particles (7° to 170° angular integration) and the hemispheric backscattered light (90° to 170°) at three wavelengths: λ = 450 nm, 550 nm and 700 nm. (Light scattered by the surrounding gas and instrument walls is subtracted.)

Particle Soot Absorption Photometer (PSAP) (*Bond et al.* 1999) The PSAP is a filter-based method used to measure in near real time light absorption (β_{abs}). In the PSAP the change in

optical transmission is measured through a filter as a function of depositing absorbing particles on the filter surface. The instruments (two in number) used in the present study, measured β_{abs} at three wavelengths: λ = 450 nm, 550 nm and 700 nm.

Multi-Angle Absorption Photometer (MAAP) (*Petzold et al.* 2004) The MAAP measures light absorption (β_{abs}) at λ = 640 nm by particles deposited on a quartz fiber filter. The absorption, which is derived from light transmission, is measured as a function of time. Additional detectors are placed at selected angles around the filter to measure and correct for light scattered by the filter surface.